Summer 7-2-2016

Synthesis, Characterization, and Pre-Ceramic Properties of π-Conjugated Polymers Based on Ni(II) Complexes of Goedken's Macrocycle

Joseph A. Paquette

Joe Gilroy
jgilroy5@uwo.ca

Synthesis, Characterization, and Pre-Ceramic Properties of π-Conjugated Polymers Based on Ni(II) Complexes of Goedken's Macrocycle

Joseph A. Paquette and Joe B. Gilroy*

Department of Chemistry and the Centre for Advanced Materials and Biomaterials Research (CAMBR), The University of Western Ontario, 1151 Richmond St. N., London, Ontario, Canada, N6A 5B7.
Correspondence to: Joe B. Gilroy (E-mail: joe.gilroy@uwo.ca)

ABSTRACT: Nickel(II) complexes of Goedken's macrocycle bearing alkyne substituents were copolymerized with 2,7-dibromo-9,9-dihexylfluorene, 2,5-dibromo-3-hexylthiophene, and 1,4-dibromo-2,5-bis(hexyloxy)benzene via microwave-induced Sonogashira cross-coupling reactions to produce copolymers **6F**, **6T**, and **6B**. The spectroscopic and electrochemical properties of the copolymers were examined and compared to model compounds. Specifically, each polymer exhibited a nickel-based absorption centered at *ca*. 589 nm and two π → π* transitions between 272 and 387 nm. While the copolymers did not exhibit extended π conjugation, the nature of the organic spacer did affect the high energy transitions. Furthermore, each copolymer underwent two ligand-based one-electron oxidations at potentials of *ca*. 0.24 V and *ca*. 0.75 V relative to the ferrocene/ferrocenium redox couple. Post-polymerization functionalization of the alkyne group in **6F** with $Co_2(CO)_8$ afforded a novel heterobimetallic copolymer that yielded amorphous nanomaterials containing Ni/Co when pyrolyzed at 800 °C for 3 h under an atmosphere of N_2/H_2 (95:5).

KEYWORDS: Metallopolymers, pyrolysis, π-conjugated polymers, metal alloys, macrocyclic ligands, post-polymerization functionalization

INTRODUCTION Metallopolymers,[1-10] which combine the processability of macromolecules and the properties of transition metals, are an intriguing class of functional materials. As a result of these combined traits, metallopolymers have been used extensively, for example, as redox-active,[11-16] magnetic,[17-22] and luminescent materials.[23-27]

The introduction of metals into π-conjugated polymer frameworks affords the ability to further expand their functionality.[28-34] One of the most well-studied classes of π-conjugated metallopolymers are metal-polyynes.[30,35-38] Wong and co-workers have previously described platinum-based systems (*e.g.*, **1**) with π-conjugation along the polymer backbone and demonstrated their utility in photovoltaic devices[37] and as pre-ceramic materials.[38-40] Another widely explored family of polymers based on π-conjugated units contain porphyrins and phthalocyanine complexes.[41-45] For example, Paik and co-workers realized a Cu(II)-containing phthalocyanine polymer (**2**) via intramolecular macrocyclization reactions in order to create single chain nanoparticles.[45] π-Conjugated metallopolymers composed of Schiff bases coordinated to transition metals have also shown widespread utility.[28,46-53] Notably, Swager and colleagues have reported polymers based on salen ligands coordinated to cobalt (*e.g.*, **3**) and demonstrated their utility as nitric oxide sensors.[48-49]

Most metallopolymers contain one metal atom in their repeating unit, which can limit their utility in some applications, including as pre-ceramic materials. The introduction of additional transition metal atoms to polymer scaffolds can afford highly metallized polymers.[38,54-58] One such example was synthesized by Manners and co-workers, where molybdenum cyclopentadienyl (Cp) carbonyl was used to append two $MoCp(CO)_2$ groups to each repeating unit of the backbone of a polyferrocenylsilane (**4**) to produce metallopolymers with utility in UV-photolithography applications.[54]

Herein, we build on our previously communicated results[59] by presenting an expansion of a series of π-conjugated polymers containing Ni(II) complexes of Goedken's macrocycle and their comprehensive characterization, including comparison to model compounds. These copolymers have been specifically

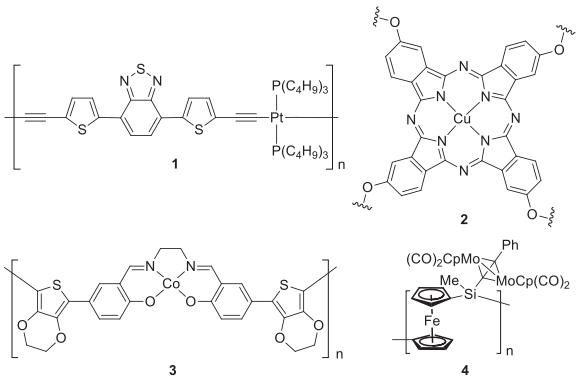

targeted in an effort to combine the redox and charge transfer properties of Ni(II)-complexes of Goedken's macrocycle[60-61] with common traits associated with π-conjugated organic polymers (*e.g.*, low band-gaps, charge transport properties).[28,35,62] Furthermore, we describe post-polymerization reactions used to transform one of the copolymers into a heterobimetallic polymer and its use as a pre-ceramic material.

EXPERIMENTAL

General Considerations

All reactions and manipulations were carried out under a nitrogen atmosphere using standard Schlenk or glove box techniques unless otherwise stated. Solvents were obtained from Caledon Laboratories, dried using an Innovative Technologies Inc. solvent purification system, collected under vacuum, and stored under a nitrogen atmosphere over 4 Å molecular sieves. Reagents were purchased from Sigma-Aldrich, Alfa Aesar, or Oakwood Chemical and used as received unless otherwise stated. 4-[(trimethylsilyl)ethynyl]-benzoyl chloride,[63] tetramethyldibenzo-tetraaza[14]annulene nickel(II),[64] 2,7-dibromo-9,9-dihexylfluorene,[65] 2-bromo-9,9-dihexylfluorene,[65] **5**,[59] **6F**,[59] **9**,[59] and **12**[59] were prepared according to previously published protocols.

NMR Spectra were recorded on a 600 MHz (^{1}H: 599.3 MHz, ^{13}C: 150.7 MHz) Varian INOVA instrument or a 400 MHz (^{1}H 400.1 MHz, ^{13}C: 100.6 MHz) Varian Mercury instrument. ^{1}H NMR spectra were referenced to residual $CHCl_3$ (7.27 ppm) and ^{13}C NMR spectra were referenced to $CDCl_3$ (77.0 ppm). Mass spectrometry data were recorded in positive-ion mode with a Bruker microTOF II instrument using electrospray ionization. UV-vis absorption spectra were recorded in CH_2Cl_2 solutions using a Cary 300 Scan instrument. Four separate concentrations were run for each sample and molar extinction coefficients were determined from the slope of a plot of absorbance against concentration. FT-IR spectra were recorded on a PerkinElmer Spectrum Two instrument using an attenuated total reflectance accessory. Powder XRD diffractograms were acquired using an Inel CPS powder diffractometer with an Inel XRG 3000 generator and Inel CPS 120 detector using a CuKα radiation source.

Microwave Reactions

Microwave reactions were carried out in a 400 W Biotage Initiator 2.0 microwave reactor. A 5 mL glass vial was charged with the relevant solid or degassed liquid reagents/solvents, sealed in an inert atmosphere glove box, and subjected to microwave irradiation as described below.

Gel Permeation Chromatography (GPC)

GPC experiments were conducted in chromatography-grade THF at concentrations of 5 mg mL^{-1} using a Viscotek GPCmax VE 2001 GPC instrument equipped with an Agilent PolyPore guard column (PL1113-1500) and two sequential Agilent PolyPore GPC columns packed with porous poly(styrene-*co*-divinylbenzene) particles (MW range: 200–2,000,000 g mol^{-1}; PL1113-6500) regulated at a temperature of 30 °C. Signal responses were measured using a Viscotek VE 3580 RI detector, and molecular weights were determined by comparison of the maximum RI response with a calibration curve (10 points, 1,500–786,000 g mol^{-1}) established using monodisperse polystyrene standards purchased from Viscotek.

Thermal Analysis and Pyrolysis Studies

Thermal degradation studies were performed using a TA Instruments Q50 TGA. Samples were placed in an alumina cup and heated at a rate of 10 °C min^{-1} from 25 to 800/1000 °C under a flow of nitrogen (60 mL min^{-1}). Differential scanning calorimetry (DSC) traces were acquired on a TA Instruments DSC Q20 instrument. The polymer samples were placed in an aluminum T_{zero} pan and heated from room temperature to 150/250 °C at 10 °C min^{-1} under a flow of nitrogen (50 mL min^{-1}) and cooled down to 0/−50 °C at 10 °C min^{-1}, before they underwent two more heating/cooling cycles.

Thin films of **6F** and **6F-[Co$_2$(CO)$_6$]$_2$** were prepared by drop-casting 250 μL of a 20 mg mL^{-1} solution of each polymer in chlorobenzene onto a silicon wafer (area = 1 cm^2). The samples were dried in air, transferred to a vacuum oven, and further dried at 60 °C for 16 h before they were heated at a rate of 10 °C min^{-1} to a temperature of 800 °C under a gentle flow of N_2/H_2 (95:5) in a quartz tube within a Lindberg Blue M tube furnace. The temperature was maintained at 800 °C for an additional 3 h before the furnace was cooled to room temperature at a rate of 10 °C min^{-1}. The samples were analyzed directly using scanning electron microscopy (SEM) at 1 keV beam energy and elemental analysis was performed at 10 keV beam energy on a LEO (Zeiss) 1540XB with an equipped Oxford X-sight X-ray detector and INCA analysis software at the Western Nanofabrication Facility.

Electrochemical Methods

Cyclic voltammetry experiments were performed with a Bioanalytical Systems Inc. (BASi) Epsilon potentiostat and analyzed using BASi Epsilon software. Typical electrochemical cells consisted of a three-electrode setup including a glassy carbon working electrode, platinum wire counter electrode, and silver wire *pseudo* reference electrode. Experiments were run at a scan rate of 100 mV s^{-1} in dry and degassed CH_2Cl_2 solutions of the analyte (~1 mM) and electrolyte (0.1 M [*n*Bu$_4$N][PF$_6$]). Cyclic voltammograms were internally referenced against the ferrocene/ferrocenium redox couple (~1 mM internal standard) and corrected for internal cell resistance using the BASi Epsilon software.

General synthetic procedure for copolymers 6F, 6T, and 6B

Compound **5** (0.10 g, 0.15 mmol), dibromoaryl monomer (0.15 mmol), $Pd(PPh_3)_4$ (0.004 g, 0.004 mmol, 10%) and CuI (0.002 g, 0.008 mmol, 5%) were combined in a microwave vial. The solvent mixture, 3 mL DMF/DIPA/H_2O (2:1:0.03), was degassed by three freeze-pump-thaw cycles, brought into a glove box and added to the solids. The reaction vessel was sealed before it was heated to 100 °C for 60 min in a microwave reactor. The resulting dark green solution was diluted with CH_2Cl_2 (20 mL), filtered and column chromatography was performed (CH_2Cl_2, 20 mL silica gel). The solvent was then removed and the resulting residue was dried overnight under vacuum. The solid was dissolved in *ca.* 2 mL CH_2Cl_2 and precipitated into diethyl ether (3 × 100 mL) and pentane (2 × 50 mL), dried, dissolved in THF (*ca*. 5 mL) and precipitated into methanol (2 × 50 mL). The resulting dark green polymers were isolated by centrifugation and dried overnight under vacuum.

Copolymer 6T

From 2,5-dibromo-3-hexylthiophene (0.050 g, 0.15 mmol). Yield = 0.075 g, 60%. ^{1}H NMR (599.3 MHz, $CDCl_3$) δ 8.23 (4H, br s, aryl C*H*), 7.72−7.70 (4H, m, aryl C*H*), 7.18 (1H, s, thiophene-C*H*), 6.67−6.62 (8H, m, aryl C*H*), 2.81−2.77 (2H, t, J_{HH} = 8 Hz, CH_2), 1.93 (12H, br s, CH_3), 1.74−1.69 (2H, m, CH_2), 1.40−1.29 (6H, m, CH_2), 0.93−0.89 (3H, m, CH_3). FT-IR (ATR): *v* = 2953 (w sh), 2926 (w), 2854 (w) 1655 (m, C=O), 1596 (m), 1527 (s), 1488 (w), 1449 (w), 1429 (m), 1362 (s), 1217 (m), 1168 (m), 1053 (w), 1013 (w), 911 (m), 852 (s), 743 (m) cm^{-1}. UV-vis (CH_2Cl_2): λ_{max} (ε) = 590 nm (5,700 M^{-1} cm^{-1}), 387 nm (74,300 M^{-1} cm^{-1}), 272 nm (45,900 M^{-1} cm^{-1}). GPC (THF, conventional calibration): M_n = 6,575 g mol^{-1}, M_w = 18,250 g mol^{-1}, *Đ* = 2.77.

Copolymer 6B

From 1,4-dibromo-2,5-bis(hexyloxy)benzene (0.066 g, 0.15 mmol). Yield = 0.081 g, 57%. ^{1}H NMR (599.3 MHz, $CDCl_3$) δ 8.22−8.15 (4H, m, aryl C*H*), 7.74-7.72 (4H, m, aryl C*H*), 7.08 (2H, s, aryl C*H*), 6.68−6.62 (8H, m, aryl C*H*), 4.11−4.00 (4H, m, OCH_2), 1.94 (12H, br. s, CH_3), 1.91−1.88 (4H, m, CH_2), 1.61−1.49 (4H, m, CH_2), 1.42−1.34 (8H, m, CH_2), 0.96−0.89 (6H, m, CH_3). FT-IR (ATR): *v* = 3407 (w, C≡C), 2949 (w sh), 2925 (w), 2856 (w) 1655 (m, C=O), 1596 (m), 1527 (s), 1429 (m), 1362 (s), 1217 (m), 1168 (m), 1053 (w), 1013 (w), 911 (m), 852 (s), 743 (m) cm^{-1}. UV-vis (CH_2Cl_2): λ_{max} (ε) = 589 nm (5,700 M^{-1} cm^{-1}), 387 nm (57,400 M^{-1} cm^{-1}), 330 nm (38,300 M^{-1} cm^{-1}), 302 (sh, 41,200 M^{-1} cm^{-1}), 272 (44,100 M^{-1} cm^{-1}). GPC (THF, conventional calibration): M_n = 7,700 g mol^{-1}, M_w = 13,600 g mol^{-1}, *Đ* = 1.76.

Synthesis of copolymer 6F-$[Co_2(CO)_6]_2$

In a glovebox, **6F** (0.10 g, 0.10 mmol) was dissolved in 5 mL dry CH_2Cl_2. $Co_2(CO)_8$ (0.09 g, 0.25 mmol) was then added to the solution, causing the immediate evolution of gas. The reaction mixture was stirred at room temperature for 30 min. Once the reaction was complete, column chromatography was performed (CH_2Cl_2, 20 mL silica gel). The solvent was removed under reduced pressure, and the residue was dissolved in *ca.* 1 mL of CH_2Cl_2 and precipitated into pentane (1 × 50 mL, then 2 × 30 mL). The solvent was then decanted and the dark green solid was dried overnight under vacuum to give **6F-$[Co_2(CO)_6]_2$** as a dark green/brown powder. Yield = 0.15 g, 95%. ^{1}H NMR (599.3 MHz, $CDCl_3$) δ 8.30−8.24 (4H, m, aryl C*H*), 7.84−7.49 (10H, m, aryl C*H*), 6.70 (4H, br. s, aryl C*H*), 6.62 (4 H, br. s, aryl C*H*), 2.00 (12H, s, CH_3), 1.94 (4H, s, CH_2), 1.33−1.08 (12H, m, CH_2), 0.90−0.71 (10H, m, CH_2, CH_3). FT-IR (ATR): *v* = 2957 (m), 2920 (m), 2853 (m) 2088 (s, C=O), 2051 (s, C=O), 2019 (s, C=O), 1725 (w), 1658 (w, C=O), 1596 (w), 1551 (m), 1454 (w), 1377 (s), 1223 (m), 1055 (m), 910 (m), 799 (m), 744 (m) cm^{-1}. UV-vis (CH_2Cl_2): λ_{max} (ε) = 587 nm (9,900 M^{-1} cm^{-1}), 385 nm (71,500 M^{-1} cm^{-1}), 270 (85,900 M^{-1} cm^{-1}). GPC (THF, conventional calibration): M_n = 7,700 g mol^{-1}, M_w = 10,900 g mol^{-1}, and *Đ* = 1.41.

Synthesis of complex 8

A Schlenk flask equipped with a stir bar was charged with complex **7** (1.68 g, 4.19 mmol), 4-[(trimethylsilyl)ethynyl]benzoyl chloride (1.00 g, 4.19 mmol) and dry toluene (100 mL) in a glove box. Upon removal, dry and degassed triethylamine (4.67 mL, 33.5 mmol) was added and the vessel was fitted with a condenser and heated to 125 °C. After stirring for 16 h, the mixture was cooled to room temperature and filtered *in vacuo*. The solvent was then removed. Column chromatography (CH_2Cl_2/Hexanes, 2:1, 100 mL silica gel) was performed to yield complex **8** as a dark green solid. Yield = 0.57 g, 23% yield (and **9**; 1.26 g, 38%. The characterization data for complex **9** were reported elsewhere).[59] ^{1}H NMR (400.1 MHz, $CDCl_3$): δ 8.15 (d, 2H, J_{HH} = 8 Hz, aryl C*H*), 7.61 (d, 2H, J_{HH} = 8 Hz, aryl C*H*), 6.72 (dd, 2H, J_{HH} =8, 1 Hz, aryl C*H*) 6.62−6.60 (m, 4H, aryl C*H*), 6.57−6.55 (m, 2H, aryl C*H*), 4.86 (s, 1H, C*H*), 2.10 (s, 6H, CH_3), 1.88 (s, 6H, CH_3), 0.28 (s, 9H, SiCH_3). ^{13}C NMR (100.6 MHz, $CDCl_3$) δ 199.5, 155.4, 153.8, 147.4, 147.2, 138.6, 132.4, 129.5, 128.1, 122.9, 121.8, 121.7, 120.9, 120.5, 111.3, 104.2, 98.3, 21.9, 20.7, −0.2. FT-IR (ATR): *v* = 2957 (w, CH), 2158 (w, C≡C), 1638 (m, C=O), 1596 (m), 1529 (s), 1453 (m), 1430 (m), 1381 (s), 1168 (m), 1215 (s), 1168 (m), 913 (m), 840 (m), 743 (m) cm^{-1}. UV-vis (CH_2Cl_2): λ_{max} (ε) 589 nm (5,500 M^{-1} cm^{-1}), 433 nm (sh, 14,100 M^{-1} cm^{-1}), 392 nm (33,400 M^{-1} cm^{-1}), 301 nm (sh, 52,800, M^{-1} cm^{-1}), 285 nm (60,800 M^{-1} cm^{-1}). Mass Spec. (ESI, +ve mode) *m/z*: $[M]^+$ calc'd for $[C_{34}H_{34}N_4NiOSi]^+$, 600.1855; found, 600.1853; difference: −0.3 ppm.

Synthesis of complex 10

Complex **8** (0.20 g, 0.33 mmol) was stirred with K_2CO_3 (0.09 g, 0.67 mmol) in THF/MeOH (3:1, 16 mL) for 16 h. CH_2Cl_2 was added and the organic layer was washed with 0.5 M

aqueous NH_4Cl (50 mL), dried with $MgSO_4$ and concentrated *in vacuo*. The resulting dark green solid was purified via precipitation from a saturated CH_2Cl_2 solution in pentane to afford **10** as a dark green microcrystalline solid. Yield = 0.14 g, 81%. ^{1}H NMR (400.1 MHz, $CDCl_3$): δ 8.18 (d, 2H, J_{HH} = 7 Hz, aryl C*H*), 7.65 (d, 2H, J_{HH} = 8 Hz, aryl C*H*), 6.73 (d, 2H, J_{HH} = 8 Hz) 6.62–6.60 (m, 4H, aryl C*H*), 6.57−6.56 (m, 2H, aryl C*H*) 4.87 (s, 1H, C*H*), 3.28 (s, 1H, C≡C-*H*), 2.10 (s, 6H, C*H*$_3$), 1.90 (s, 6H, C*H*$_3$). ^{13}C NMR (100.6 MHz, $CDCl_3$) δ 199.4, 155.4, 153.8, 147.4, 147.1, 139.0, 132.6, 129.5, 127.0, 123.0, 121.8, 121.7, 120.9, 120.4, 111.2, 82.9, 80.5, 21.9, 20.7. FT-IR (ATR): *v* = 3301 (w), 1663 (w, C=O), 1597 (w), 1530 (m), 1454 (m), 1429 (m), 1382 (s), 1365 (s), 1217 (m), 1166 (m), 1054 (m), 913 (m), 853 (s), 772 (m), 746 (s), 645 (m), 617 (m) cm^{-1}. UV-vis (CH_2Cl_2): λ_{max} (ε) 588 nm (4,100 M^{-1} cm^{-1}), 427 nm (sh, 9,200 M^{-1} cm^{-1}), 392 nm (23,700 M^{-1} cm^{-1}), 274 nm (33,700 M^{-1} cm^{-1}). Mass Spec. (ESI, +ve mode) *m/z*: [M]$^+$ calc'd for $[C_{31}H_{26}N_4NiO]^+$, 528.1460; found, 528.1452; difference: −1.5 ppm.

Synthesis of model compound 11

Compound **10** (0.11 g, 0.21 mmol), 2,7-dibromo-9,9-dihexylfluorene (0.05 g, 0.10 mmol), $Pd(PPh_3)_4$ (0.006 g, 0.005 mmol) and CuI (2.0 g, 0.011 mmol) were combined in a 5 mL microwave vial. The solvent mixture, 3 mL DMF/DIPA/H_2O (2:1:0.03) was degassed by 3 freeze-pump-thaw cycles, brought into a glove box and added to the solid. The microwave vial was sealed and then heated at 100 °C for 45 min in a microwave reactor. Upon cooling, CH_2Cl_2 (10 mL) was added to the dark green solution and the entire mixture washed with H_2O (6 × 100 mL), dried with $MgSO_4$ and concentrated *in vacuo*. The resulting dark green residue was purified using a column chromatography (CH_2Cl_2, 25 mL silica gel) to afford **11** as a dark green microcrystalline solid after solvent removal *in vacuo*. Yield = 0.12 g, 83%. ^{1}H NMR (599.4 MHz, $CDCl_3$): δ 8.23 (d, 4H, $^3J_{HH}$ = 8 Hz, aryl C*H*), 7.72 (m, 6H, aryl C*H*), 7.59-7.54 (m, 2H, aryl C*H*), 7.56 (s, 2H, aryl C*H*), 6.74 (m, 4H, aryl C*H*), 6.67–6.61 (m, 8H, aryl C*H*), 6.58–6.56 (m, 4H, aryl C*H*), 4.89 (s, 2H, C*H*), 2.12 (s, 12H, C*H*$_3$) 2.04−2.01 (m, 4H, C*H*$_2$), 1.94 (s, 12H, C*H*$_3$), 1.16–1.05 (m, 12H, C*H*$_2$), 0.78 (t, 6H, $^3J_{HH}$ = 8 Hz, C*H*$_3$), 0.68−0.63 (m, 4H, C*H*$_2$). ^{13}C NMR (150.7 MHz, $CDCl_3$): δ 199.5, 155.4, 153.9, 151.3, 147.4, 147.2, 141.1, 138.4, 132.0, 131.0, 129.7, 128.5, 126.1, 122.9, 121.9, 121.8, 121.5, 120.9, 120.6, 120.2, 111.3, 94.0, 89.3, 55.4, 40.4, 31.5, 29.7, 23.7, 22.6, 21.9, 20.7, 14.0. FT-IR (ATR): *v* = 2952 (s, hex CH), 2923 (s, hex CH), 2852 (s, hex CH), 1631 (m, C=O), 1595 (m), 1527 (s), 1454 (m), 1430 (m), 1381 (s), 1215 (m), 1051 (m), 1022 (m), 912 (m), 853 (m), 819 (m), 742 (m) cm^{-1}. UV-vis (CH_2Cl_2): λ_{max} (ε) = 584 nm (7,900 M^{-1} cm^{-1}), 387 nm (91,100 M^{-1} cm^{-1}), 273 nm (52,100 M^{-1} cm^{-1}). Mass Spec. (ESI, +ve mode) *m/z*: [M + H]$^+$ calc'd for $[C_{87}H_{83}N_8Ni_2O_2]^+$, 1387.5346; found, 1387.5365; difference: +1.4 ppm.

RESULTS AND DISCUSSION

Copolymer Synthesis

Polymers (**6F**, **6T**, and **6B**) containing 9,9-dihexylfluorene (**F**), 3-hexylthiophene (**T**), or 2,5-bis(hexyloxy)benzene (**B**) and a Ni(II) complex of Goedken's macrocycle (**5**) were synthesized using previously optimized polymerization conditions (Scheme 1).[59] These comonomers were chosen for polymerization due to their π-conjugated nature and ability to potentially solubilize the rigid, π-conjugated backbones of the targeted copolymers (Scheme 1). The monomers were combined in equimolar quantities and dissolved in a dimethylformamide (DMF), di-*iso*propylamine (DIPA), and water mixture (2:1:0.03). Sonogashira cross-coupling polymerization was performed using a catalytic amount of tetrakis(triphenylphosphine) palladium (2.5%) and copper iodide (5.0%) submitted to microwave irradiation for 60 min at 100 °C. Purification of the polymers involved column chromatography to remove catalyst, removal of the majority of DMF and DIPA *in vacuo* and precipitation in diethyl ether from CH_2Cl_2, in pentane from CH_2Cl_2 (2 × 50 mL), and in MeOH (2 × 50 mL) from THF, in order to remove shorter molecular weight oligomers as well as residual DIPA and DMF. The isolated yields for copolymers **6F**, **6T**, and **6B** were 59, 60, and 57% respectively, and a summary of the molecular weight data acquired by gel permeation chromatography (GPC) can be found in Table 1. The relatively low molecular weights and broad molecular weight distributions observed are consistent with the step-growth polymerization method employed. Additional details,

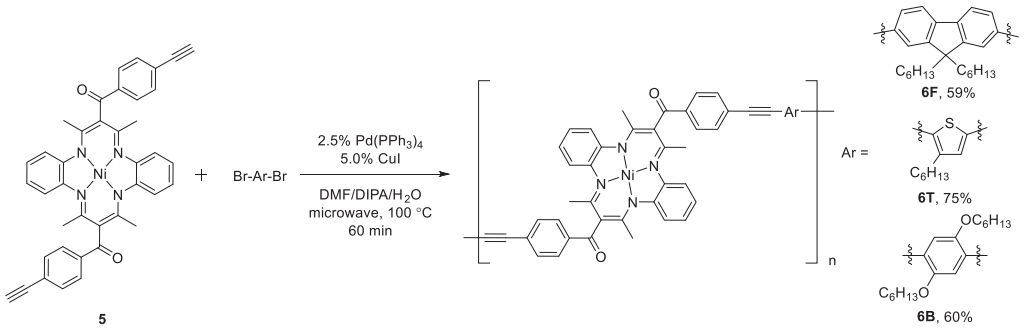

SCHEME 1 Synthesis of copolymers **6F**, **6B**, and **6T**.

TABLE 1 Summary of GPC data for copolymers **6F**, **6F-[$Co_2(CO)_6$]$_2$**, **6B**, and **6T**.

Compound	M_n (g mol^{-1})	M_w (g mol^{-1})	$Đ$
6F	7,825	11,800	1.51
6F-[$Co_2(CO)_6$]$_2$	7,700	10,900	1.41
6T	6,575	18,250	2.77
6B	7,700	13,600	1.76

including thermal analysis and spectroscopic data are discussed below (Figures S1, S2).

Model Compound Synthesis

In order to gain further insight into the spectroscopic properties of the copolymers, specifically **6F**, model compounds **11** and **12** were prepared via similar Sonogashira cross-coupling reactions (Scheme 2). The first model compound consisted of two Ni(II) complexes of Goedken's macrocycles bridged by a 9,9-dihexylfluorene molecule (**11**). The second model compound consisted of two 9,9-dihexylfluorene molecules bridged by a single Ni(II) complex of Goedken's macrocycle (**12**). To synthesize compound **11**, access to a Ni(II) complex of Goedken's macrocycle substituted with a single alkyne functionality was required. Thus, a mixture of 4-[(trimethylsilyl)ethynyl]-benzoyl chloride and compound **7** was heated to reflux in the presence of triethylamine (Scheme 2). This reaction afforded a mixture of mono- (**8**) and di-substituted (**9**) macrocycles which could be separated using column chromatography, in 23 and 38% yield, respectively. The identity of complex **8** was confirmed by NMR spectroscopy (Figures S3, S4). Removal of the TMS group from compounds **8** and **9** was achieved using potassium carbonate to afford compounds **10** and **5** in 81 and 90% yield, respectively (Figures S5, S6).

Microwave irradiation of a mixture of two equiv. of **10** with one equiv. of 2,7-dibromo-9,9-dihexylfluorene for 30 min at 100 °C in the presence of $Pd(PPh_3)_4$ and CuI dissolved in DMF/DIPA/H_2O (2:1:0.03) produced compound **11** in 83% yield after purification by column chromatography (Figures S7, S8).

TABLE 2 UV-vis absorption spectroscopy data for copolymers **6F**, **6F-[$Co_2(CO)_6$]$_2$**, **6T**, and **6B**, and model compounds **11** and **12** in CH_2Cl_2.

Compound	λ_{max} (nm), ε (M^{-1} cm^{-1})		
	π → π*$_1$	π → π*$_2$	LMCT[a]
6F[59]	275, 50,900	378, 100,800	588, 6,000
6F-[$Co_2(CO)_6$]$_2$	270, 85,900	385, 71,500	587, 9,900
6T	272, 45,900	387, 74,300	590, 5,700
6B	272, 44,100	387, 57,400	589, 5,700
11	273, 52,100	387, 91,100	584, 7,900
12[59]	283, 67,600	349, 109,200	587, 7,100

[a]Ligand-to-metal charge transfer.

UV-vis Absorption Spectroscopy

The UV-vis absorption spectra of polymers **6F**, **6T**, and **6B** are presented in Figure 1a and the spectral features summarized in Table 2. The spectra of polymers **6T** and **6B** showed absorption maxima at 272 nm (**6T**, ε = 45,900 and **6B**, ε = 44,100 M^{-1} cm^{-1}), 387 nm (**6T**, ε = 74,300 and **6B**, ε = 57,400 M^{-1} cm^{-1}) and similar low-energy absorption maxima at *ca.* 590 nm (5,700 M^{-1} cm^{-1}). Similarly, polymer **6F** yielded absorption maxima at 275 nm (50,900 M^{-1} cm^{-1}), 378 nm (100,800 M^{-1} cm^{-1}), and 588 nm (6,000 M^{-1} cm^{-1}). The low energy absorption has been previously assigned in molecular analogues to a charge transfer from the highest ligand occupied molecular orbital of the macrocyclic backbone to the lowest empty d orbital of Ni(II).[66] It was observed that the absorption at *ca.* 590 nm remains essentially unchanged in the copolymers due to the lack of long range electronic delocalization via the orthogonal arrangement of the Ni(II) macrocycle units and the organic spacers, as previously inferred by the solid-state

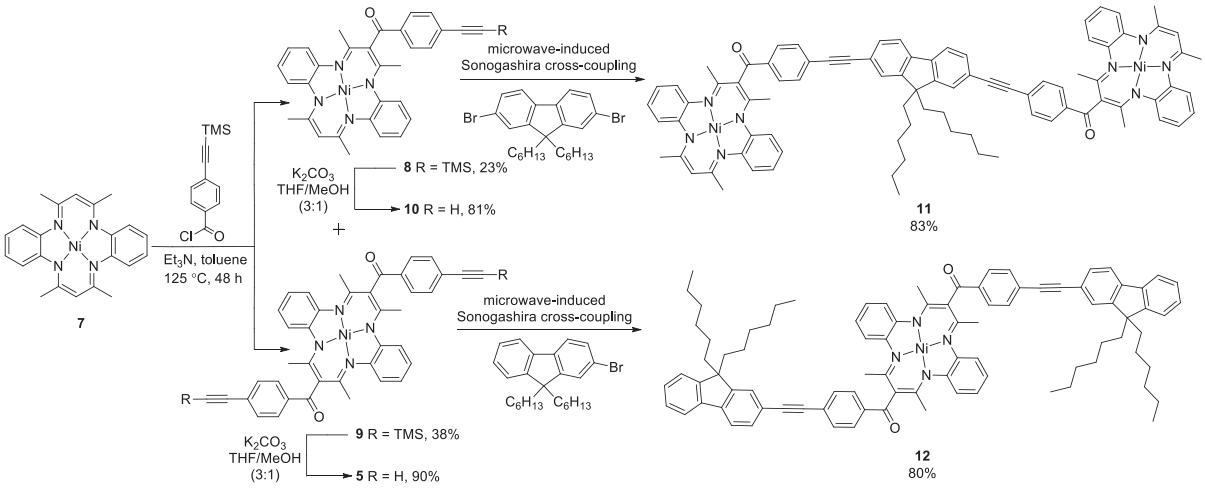

SCHEME 2 Synthesis of model compounds **11** and **12**.

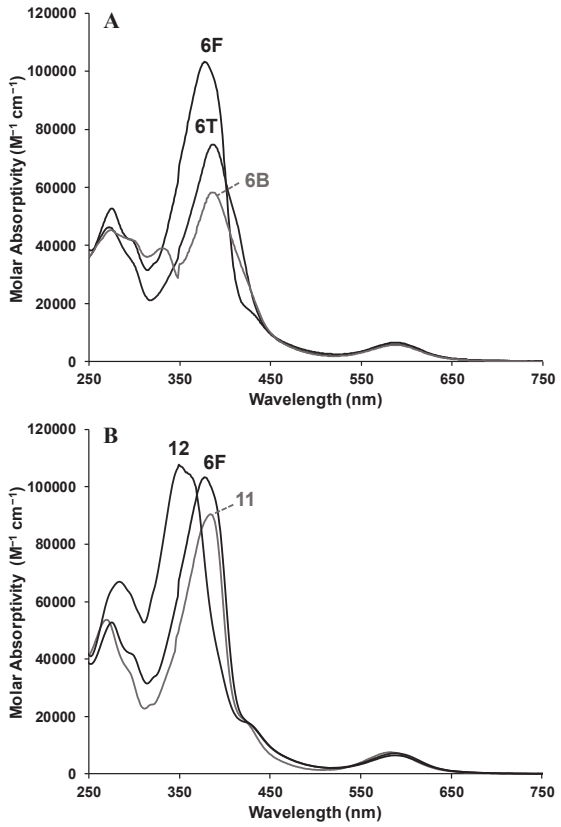

FIGURE 1 UV-vis absorption spectra recorded in CH_2Cl_2. A) Comparison of copolymers **6F**, **6T**, and **6B**. B) Comparison of model compounds **11**, **12**, and copolymer **6F**.

structure of **5**.[59] The high-energy absorptions at *ca.* 272 nm is thought to be a π → π* transition associated with Goedken's macrocycle, while the transition at *ca.* 387 nm appears to originate primarily from a macrocycle centered π → π* transition associated with the π-conjugated organic spacer in each structure. The π → π^*_2 transition of copolymer **6F** is blue-shifted by *ca.* 10 nm compared to these of copolymers **6T** and **6B**. This trend is consistent with that observed for the wavelengths of maximum absorption of poly(9,9-dihexylfluorene) and poly(3-hexylthiophene) and may relate to the antiaromatic nature of the 9,9-dihexylfluorene spacer.[67-68]

In order to further understand the absorption properties of the copolymers, the absorption behavior of model complexes **11** and **12** were examined. Model compound **11**, which contains two Ni(II) complexes bridged by a 9,9-dihexylfluorene, shows absorption maxima at 584, 387, and 273 nm (Figure 1b). Model compound **12**, which contains two fluorene molecules and one Ni(II) complex, shows absorbance maxima at 587, 349, and 283 nm. The intermediate absorption maxima at 349 nm was blue-shifted with respect to **6F** and **11,** which both had maximum absorptions at 387 nm. This is thought to be due to the presence of a shorter conjugated π-system [CO-Ph-alkyne-(9,9-dihexylfluorene)] within the backbone in compound **12**, compared to the relatively large CO-Ph-alkyne-(9,9-dihexylfluorene)-alkyne-Ph-CO system present in model compound **11** and copolymer **6F**. The increase in π-conjugation accounts for ten additional π-electrons and results in a red-shift in λ_{max} of 38 nm. The Ni(II) based absorption at *ca.* 590 nm for **11**, **12**, and **6F** were unchanged regardless of the degree of π-conjugation within the organic spacer (Table 2).

Cyclic Voltammetry

The electrochemical properties of polymers **6F**, **6T**, and **6B** are summarized in Table 3. Cyclic voltammetry studies of the copolymers revealed two reversible one-electron oxidation events at $E°_{ox1}$ = 0.24 and $E°_{ox2}$ = 0.74 V for **6F**, $E°_{ox1}$ = 0.23 and $E°_{ox2}$ = 0.74 V for **6T**, and $E°_{ox1}$ = 0.25 and $E°_{ox2}$ = 0.75 V for **6B** in CH_2Cl_2, relative to the ferrocene/ferrocenium redox couple (Figure 2). Model compound **12** also produced two reversible one-electron oxidation waves at $E°_{ox1}$ = 0.25 and $E°_{ox2}$ = 0.76 V (Figure S9). The electrochemical behavior of model compound **11** was considerably more complicated, although similar to other unsubstituted Ni(II) complexes of Goedken's macrocycle (Figure S10).[66] Compound **11** gave rise to three irreversible oxidation waves at $E_{pa(1)}$ = 0.16 V, $E_{pa(2)}$ = 0.92 V, and $E_{pa(3)}$ = 1.11 V and a single irreversible reduction

TABLE 3 Cyclic voltammetry data for polymers **6F**, **6T**, **6B** and model compounds **11** and **12**.[a]

Compounds	$E_{pa(1)}$[b]	$E°_{ox1}$	$E_{pc(1)}$[c]	$E°_{ox2}$	$E_{pa(2)}$[b]	$E_{pa(3)}$[b]
6F[59]	-	0.24	-	0.74	-	-
6T	-	0.23	-	0.74	-	-
6B	-	0.25	-	0.75	-	-
11	0.16	-	0.74	-	0.92	1.11
12[59]	-	0.25	-	0.76	-	-

[a] Recorded at a scan rate of 100 mV s^{-1} in a CH_2Cl_2 solution containing 1 × 10^{-3} M analyte and 0.1 M [nBu$_4$N][PF_6] as supporting electrolyte. Potentials reported in V relative to the ferrocene/ferrocenium redox couple.
[b] Irreversible process, anodic peak potential (E_{pa}) reported.
[c] Irreversible process, cathodic peak potential (E_{pc}) reported.

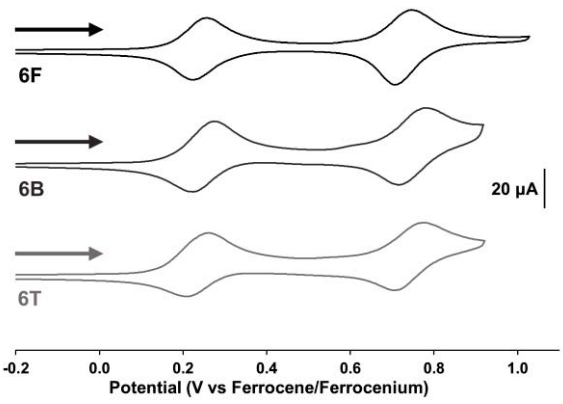

FIGURE 2 Cyclic voltammagrams of **6F**, **6T**, and **6B** recorded at a scan rate of 100 mV s^{-1} in CH_2Cl_2 solutions containing 1 × 10^{-3} M analyte and 0.1 M [nBu$_4$N][PF_6] as supporting electrolyte.

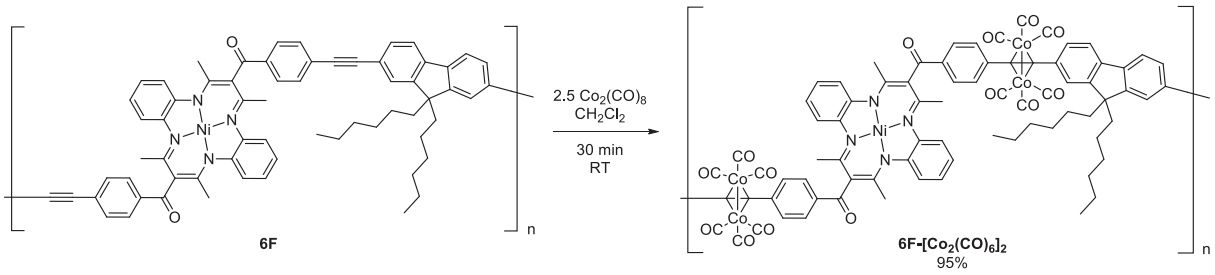

SCHEME 3 Synthesis of **6F-[Co₂(CO)₆]₂**.

wave $E_{pc(1)}$ = 0.74 V. The irreversible oxidation at 1.11 V has been reported to arise due to the oxidation of a dimer formed via radical coupling of two equivalents of the radical cation form of similar Ni(II) complexes of Goedken's macrocycle.[69]

Furthermore, Ni(II) complexes of Goedken's macrocycle have been shown to form polymeric species on electrode surfaces.[70] Upon cycling repeatedly between 0.0 and 1.3 V, film formation was observed in the case of **11**, but there was a lack of current enhancement typically associated with electropolymerization (Figure S11).[28] Rather, we presume that a variety of oligomeric species are generated upon oxidation, leading to similar oxidation events (E = 0.6−0.9 V) and electrode plating being observed.[71]

Post-Polymerization Functionalization

In order to produce a heterobimetallic copolymer, **6F** was dissolved in CH_2Cl_2 and reacted with 2.5 equiv. of $Co_2(CO)_8$. The resulting copolymer was purified using flash column chromatography on alumina and repeated precipitations from CH_2Cl_2 into pentane, to afford **6F-[Co₂(CO)₆]₂** in 95% yield (Scheme 3). GPC analysis of **6F-[Co₂(CO)₆]₂** yielded M_n = 7,700 g mol^{-1}, M_w = 10,900 g mol^{-1}, and $Đ$ = 1.41. The overall distribution and shape of the GPC traces are conserved when compared to the original polymer **6F** (Figure S12), which suggests the integrity of the polymer backbone was maintained after the introduction of the cobalt carbonyl clusters.

UV-vis absorption spectroscopy confirmed the preservation of the absorption maxima at 587, 385, and 270 nm when compared to the parent polymer **6F** (Figure S13), although the molar absorptivity of the absorption maxima at 385 nm was reduced from ε = 100,800 M^{-1} cm^{-1} in **6F** to ε = 71,500 M^{-1} cm^{-1} in **6F-[Co₂(CO)₆]₂** and the molar absorptivity of the absorption maxima at 275 nm was increased from ε = 50,900 M^{-1} cm^{-1} in **6F** to ε = 85,900 M^{-1} cm^{-1} in **6F-[Co₂(CO)₆]₂**. Furthermore, analysis of the FT-IR spectrum of **6F-[Co₂(CO)₆]₂** revealed the appearance of three diagnostic carbonyl stretches at 2019, 2051, and 2088 cm^{-1}, and the disappearance of the alkyne C≡C stretch at 2196 cm^{-1} (Figure 3). ^{1}H NMR spectroscopy revealed similar chemical shifts for most of the proton signals present in **6F** and **6F-[Co₂(CO)₆]₂** copolymers, although there was a significant difference for some of the chemical shifts of the signals corresponding to the protons present on the fluorene organic spacer, including the aromatic and aliphatic signals (Figure S14).

Thermal Analysis

Thermal gravimetric analysis (TGA) of copolymers **6F**, **6T**, and **6B** demonstrated their thermal stability up to temperatures

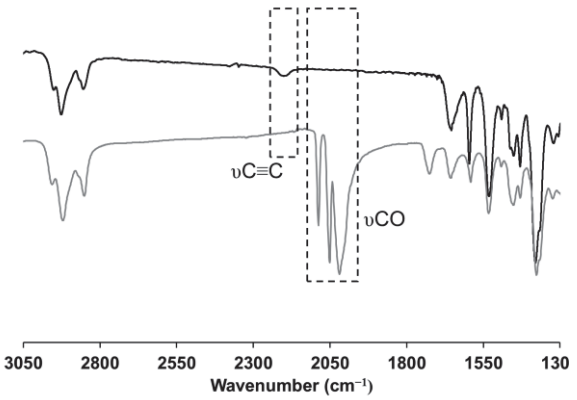

FIGURE 3 FT-IR spectra of **6F** (black) and **6F-[Co₂(CO)₆]₂** (grey). The dashed boxes highlight the energy regions of specific interest.

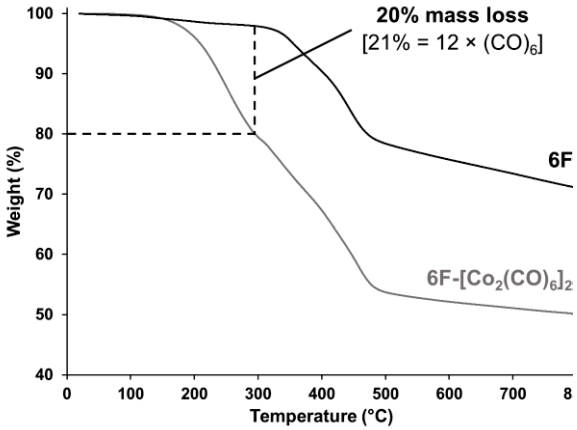

FIGURE 4 TGA data demonstrating the thermal decomposition of **6F** (black) and **6F-[Co₂(CO)₆]₂** (grey).

of 316, 284, and 252 °C, respectively (Figures 4, S15, and S16). Differential scanning calorimetry studies did not reveal glass transitions between 0 and 250 °C (Figures S17−S19). We speculate that the lack of observable glass transitions may be attributed to interdigitation of the alkyl chains present on the backbones of these polymers.

TGA data collected for copolymer **6F-[Co$_2$(CO)$_6$]$_2$** showed its thermal stability up to 177 °C before decomposition occurred in two steps. The first decomposition occurred to a temperature of *ca.* 300 °C with an initial mass loss of *ca.* 20%. This mass loss accounts for the expulsion of the carbonyl groups present on the polymer backbone, which corresponds to 21% of the total polymer mass. The second step resulted in a further mass loss of 46% to a temperature of 490 °C, and was followed by a slow thermal degradation until a char yield of 50% was achieved at 800 °C (Figure 4). For comparison, the char yield observed for **6F** was *ca*. 70%. Upon inspection of the TGA data for **6F** and **6F-[Co$_2$(CO)$_6$]$_2$**, there were similar degradation features after the initial loss of the carbonyl groups once the thermal stability limit was reached at 316 °C. The DSC data for **6F-[Co$_2$(CO)$_6$]$_2$** did not reveal a glass transition within the stability window of the polymer (Figure S20).

Pre-Ceramic Properties

The interesting thermal decomposition characteristics and significant char yields (> 50%) observed for **6F** and **6F-[Co$_2$(CO)$_6$]$_2$** suggested the formation of potentially useful ceramic materials. Specifically, Ni/Co alloys were targeted due to their demonstrated utility as magnetic materials,[72] their use in catalysis,[73-74] and their high charge capacity.[75] Thin-films of **6F** and **6F-[Co$_2$(CO)$_6$]$_2$**, estimated to be approximately 5 µm thick (Figure S21), were created by drop-casting a 20 mg mL^{-1} solution of each polymer in chlorobenzene onto a silicon wafer. The loaded wafers were then dried overnight in a vacuum oven at 60 °C before the samples were heated to 800 °C at a rate of

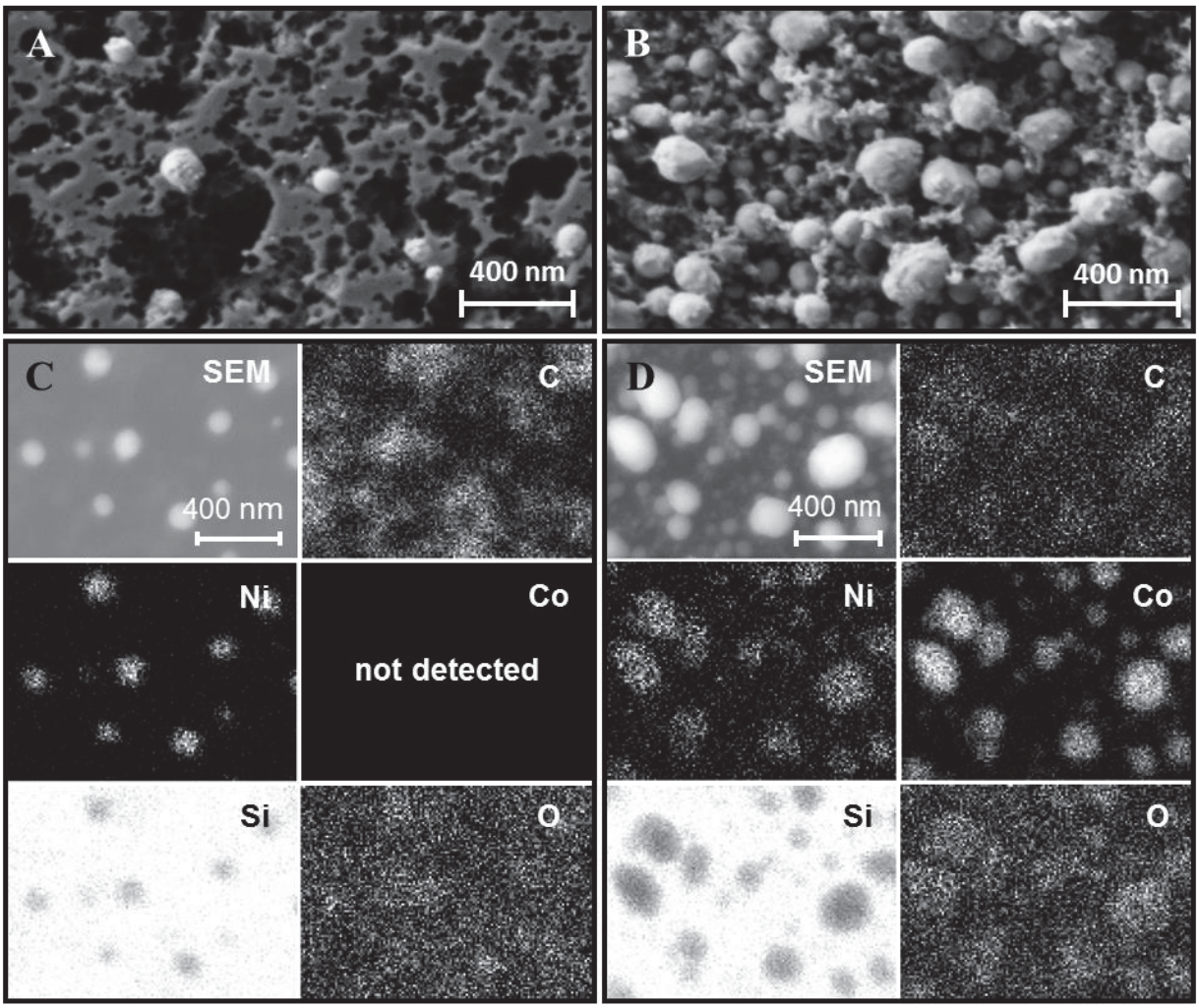

FIGURE 5 Scanning electron micrographs of the nanomaterials resulting from pyrolysis of A) **6F** and B) **6F-[Co$_2$(CO)$_6$]$_2$**. Elemental maps (EDX spectroscopy) of the nanomaterials resulting from the pyrolysis of C) **6F** and D) **6F-[Co$_2$(CO)$_6$]$_2$**. Light areas indicate a positive response for the elements in question.

10 °C min^{-1} and held at that temperature for an additional 3 h under a N_2/H_2 (95:5) atmosphere. Upon cooling, the samples were studied using scanning electron microscopy (SEM) and energy-dispersive X-ray (EDX) spectroscopy.

SEM images of the pyrolyzed films of **6F** and **6F-[$Co_2(CO)_6$]$_2$** are shown in Figure 5. The micrographs of the nanomaterials derived from **6F** show the presence of ill-defined nanoparticles within a porous matrix. Based on our EDX spectroscopy analysis we conclude that the nickel-rich nanoparticles are suspended in a porous and amorphous carbon matrix, presumably carbon black (Figures 5a, c). Oxygen appeared throughout the film and was concentrated in metal-rich areas. Although the pyrolysis experiments were performed in the absence of oxygen, brief exposure likely led to the formation of a thin layer of nickel-oxide. The micrograph of the nanomaterials that resulted from the pyrolysis of **6F-[$Co_2(CO)_6$]$_2$** showed a surface more densely populated with metallic nanoparticles within an amorphous carbon matrix (Figure 5b). The nanoparticles were shown to be rich in cobalt and nickel (Figure 5d), while the cobalt and nickel alloys appeared to be more susceptible to oxidation based on the elemental maps obtained (Figure 5d). Furthermore, the ratio of cobalt to nickel (*ca*. 5.5:1) was measured by EDX spectroscopy, which deviated from the 4:1 ratio of metals present in **6F-[$Co_2(CO)_6$]$_2$** (Figure S22). Powder X-ray diffraction studies of the pyrolyzed thin-films of **6F** and **6F-[$Co_2(CO)_6$]$_2$** indicated the presence of amorphous materials, consistent with the morphologies observed using SEM. These studies demonstrated our ability, through post-polymerization functionalization, to control the ratio of metals present within the nanomaterials.

CONCLUSIONS

Nickel(II) complexes of Goedken's macrocycle bearing alkyne substituents were copolymerized with 2,7-dibromo-9,9-dihexylfluorene, 2,5-dibromo-3-hexylthiophene, and 1,4-dibromo-2,5-bis(hexyloxy)benzene via a microwave-induced Sonogashira cross-coupling reaction to produce copolymers **6F**, **6T**, and **6B**. The copolymers exhibited high thermal stability (up to 300 °C) and two one-electron oxidation waves in their cyclic voltammograms. The spectroscopic properties of copolymer **6F** were probed by comparison with model compounds **11** and **12**, which provided insight into the observed spectroscopic properties for this family of copolymers. Specifically, the intermediate absorption maxima observed for the copolymers was shown to vary with the size and nature of the organic spacer within the polymer backbones. Post-polymerization functionalization via the alkyne synthetic handle present in **6F** led to the production of heterobimetallic copolymers that produced interesting amorphous nanomaterials rich in nickel and cobalt upon pyrolysis, with metal content influenced by the structure of the polymer.

ACKNOWLEDGEMENTS

We would like to thank the University of Western Ontario, the Natural Science and Engineering Research Council (NSERC) of Canada (J. B. G.: DG, 435675 and J. A. P.: PGS D scholarship), the Ontario Ministry of Training, Colleges and Universities (J.A.P.: Ontario Graduate Scholarship) the Ontario Ministry of Research and Innovation (J. B. G.: ERA, ER14-10-147) and the Canada Foundation for Innovation (J. B. G.: JELF, 33977) for funding this work. We thank Profs. Elizabeth R. Gillies, Michael A. Kerr, and Paul J. Ragogna for access to instrumentation in their labs. Finally, we acknowledge Dr. Todd Simpson and Tim Goldhawk at the Western Nanofabrication Facility and Amir Rabiee Kenaree for their assistance with SEM and EDX spectroscopy studies.

REFERENCES AND NOTES

1 Y. Lu, N. Yeung, N. Sieracki, N. M. Marshall, *Nature* **2009**, *460*, 855−862.

2 C.-L. Ho, W.-Y. Wong, *Coord. Chem. Rev.* **2011**, *255*, 2469−2502.

3 G. R. Whittell, M. D. Hager, U. S. Schubert, I. Manners, *Nat. Mater.* **2011**, *10*, 176−188.

4 B. Bagh, J. B. Gilroy, A. Staubitz, J. Muller, *J. Am. Chem. Soc.* **2010**, *132*, 1794−1795.

5 Y. Zha, H. D. Thaker, R. R. Maddikeri, S. P. Gido, M. T. Tuominen, G. N. Tew, *J. Am. Chem. Soc.* **2012**, *134*, 14534−14541.

6 X. Wang, K. Cao, Y. Liu, B. Tsang, S. Liew, *J. Am. Chem. Soc.* **2013**, *135*, 3399−3402.

7 M. Hadadpour, Y. Liu, P. Chadha, P. J. Ragogna, *Macromolecules* **2014**, *47*, 6207−6217.

8 G. M. Pawar, R. A. Lalancette, E. M. Bonder, J. B. Sheridan, F. Jäkle, *Macromolecules* **2015**, *48*, 6508−6515.

9 B. Sandmann, B. Happ, S. Kupfer, F. H. Schacher, M. D. Hager, U. S. Schubert, *Macromol. Rapid Commun.* **2015**, *36*, 604−609.

10 Y. Yan, J. Zhang, L. Ren, C. Tang, *Chem. Soc. Rev.* **2016**, 10.1039/C36CS00026F.

11 X. Feng, K. Zhang, M. A. Hempenius, G. J. Vancso, *RSC Adv.* **2015**, *5*, 106355−106376.

12 R. Rulkens, A. J. Lough, I. Manners, S. R. Lovelace, C. Grant, W. E. Geiger, *J. Am. Chem. Soc.* **1996**, *118*, 12683−12695.

13 Y. Ma, W.-F. Dong, M. A. Hempenius, H. Möhwald, G. J. Vancso, *Nat. Mater.* **2006**, *5*, 724−729.

14 R. H. Staff, M. Gallei, M. Mazurowski, M. Rehahn, R. Berger, K. Landfester, D. Crespy, *ACS Nano* **2012**, *6*, 9042−9049.

15 A. Rabiee Kenaree, B. M. Berven, P. J. Ragogna, J. B. Gilroy, *Chem. Commun.* **2014**, *50*, 10714−10717.

16 K. Zhang, X. Feng, X. Sui, M. A. Hempenius, G. J. Vancso, *Angew. Chem. Int. Ed.* **2014**, *53*, 13789−13793.

17 M. J. MacLachlan, M. Ginzburg, N. Coombs, T. W. Coyle, N. P. Raju, J. E. Greedan, G. A. Ozin, I. Manners, *Science* **2000**, *287*, 1460−1463.

18 T. J. O'Sullivan, B. Djukic, P. A. Dube, M. T. Lemaire, *Chem. Commun.* **2009**, 1903−1905.

19 Z. M. Al-Badri, R. R. Maddikeri, Y. Zha, H. D. Thaker, P. Dobriyal, R. Shunmugam, T. P. Russell, G. N. Tew, *Nat. Commun.* **2011**, *2*, 482.

20 S. Baljak, A. D. Russell, S. C. Binding, M. F. Haddow, D. O'Hare, I. Manners, *J. Am. Chem. Soc.* **2014**, *136*, 5864−5867.

21 H. Braunschweig, A. Damme, S. Demeshko, K. Dück, T. Kramer, I. Krummenacher, F. Meyer, K. Radacki, S. Stellwag-Konertz, G. R. Whittell, *J. Am. Chem. Soc.* **2015**, *137*, 1492−1500.

22 B. Jiang, W. L. Hom, X. Chen, P. Yu, L. C. Pavelka, K. Kisslinger, J. B. Parise, S. R. Bhatia, R. B. Grubbs, *J. Am. Chem. Soc.* **2016**, *138*, 4616−4625.

23 C. Ulbricht, B. Beyer, C. Friebe, A. Winter, U. S. Schubert, *Adv. Mater.* **2009**, *21*, 4418−4441.

24 C. Ulbricht, C. R. Becer, A. Winter, U. S. Schubert, *Macromol. Rapid Commun.* **2010**, *31*, 827−833.

25 A. M. Soliman, D. Fortin, E. Zysman-Colman, P. D. Harvey, *Macromol. Rapid Commun.* **2012**, *33*, 522−527.

26 A. Wild, A. Teichler, C.-L. Ho, X.-Z. Wang, H. Zhan, F. Schlütter, A. Winter, M. D. Hager, W.-Y. Wong, U. S. Schubert, *J. Mater. Chem. C* **2013**, *1*, 1812−1822.

27 Y. Matsumura, K. Fukuda, S. Inagi, I. Tomita, *Macromol. Rapid Commun.* **2015**, *36*, 660−664.

28 B. J. Holliday, T. M. Swager, *Chem. Commun.* **2005**, 23−36.

29 C. Moorlag, B. C. Sih, T. L. Stott, M. O. Wolf, *J. Mater. Chem.* **2005**, *15*, 2433−2436.

30 W.-Y. Wong, P. D. Harvey, *Macromol. Rapid Commun.* **2010**, *31*, 671−713.

31 C. Friebe, M. D. Hager, A. Winter, U. S. Schubert, *Adv. Mater.* **2012**, *24*, 332−345.

32 K. R. Edelman, K. J. Stevenson, B. J. Holliday, *Macromol. Rapid Commun.* **2012**, *33*, 610−615.

33 C. Friebe, B. Schulze, H. Görls, M. Jäger, U. S. Schubert, *Chem. Eur. J.* **2014**, *20*, 2357−2366.

34 J. D. Caraway, M. T. Nguyen, L. A. Mitchell, B. J. Holliday, *Macromol. Rapid Commun.* **2015**, *36*, 665−670.

35 W.-Y. Wong, C.-L. Ho, *Acc. Chem. Res.* **2010**, *43*, 1246−1256.

36 M. Yang, L. Zhang, Z. Lei, P. Ye, J. Si, Q. Yang, Y. Wang, *J. Appl. Polym. Sci.* **1998**, *70*, 1165−1172.

37 W.-Y. Wong, X.-Z. Wang, Z. He, A. B. Djurišić, C.-T. Yip, K.-Y. Cheung, H. Wang, C. S. K. Mak, W.-K. Chan, *Nat. Mater.* **2007**, *6*, 521−527.

38 C.-L. Ho, S.-Y. Poon, K. Liu, C.-K. Wong, G.-L. Lu, S. Petrov, I. Manners, W.-Y. Wong, *J. Organomet. Chem.* **2013**, *744*, 165−171.

39 Q. Dong, G. Li, C.-L. Ho, M. Faisal, C.-W. Leung, P. W.-T. Pong, K. Liu, B.-Z. Tang, I. Manners, W.-Y. Wong, *Adv. Mater.* **2012**, *24*, 1034−1040.

40 K. Liu, C.-L. Ho, S. Aouba, Y.-Q. Zhao, Z.-H. Lu, S. Petrov, N. Coombs, P. Dube, H. E. Ruda, W.-Y. Wong, I. Manners, *Angew. Chem. Int. Ed.* **2008**, *47*, 1255−1259.

41 E. Scamporrino, D. Vitalini, *Macromolecules* **1992**, *25*, 1625−1632.

42 H. Eichhorn, M. Sturm, D. Wöhrle, *Macromol. Chem. Phys.* **1995**, *196*, 115−131.

43 X. Ding, J. Guo, X. Feng, Y. Honsho, J. Guo, S. Seki, P. Maitarad, A. Saeki, S. Nagase, D. Jiang, *Angew. Chem. Int. Ed.* **2011**, *50*, 1289−1293.

44 M. Abel, S. Clair, O. Ourdjini, M. Mossoyan, L. Porte, *J. Am. Chem. Soc.* **2011**, *133*, 1203−1205.

45 J. Jeong, Y.-J. Lee, B. Kim, B. Kim, K.-S. Jung, H.-j. Paik, *Polym. Chem.* **2015**, *6*, 3392−3397.

46 A. C. W. Leung, M. J. MacLachlan, *J. Inorg. Organomet. Polym. Mater.* **2007**, *17*, 57−89.

47 R. P. Kingsborough, T. M. Swager, *Chem. Mater.* **2000**, *12*, 872−874.

48 T. Shioya, T. M. Swager, *Chem. Commun.* **2002**, 1364−1365.

49 B. J. Holliday, T. B. Stanford, T. M. Swager, *Chem. Mater.* **2006**, *18*, 5649−5651.

50 H. Fukumoto, K. Yamane, Y. Kase, T. Yamamoto, *Macromolecules* **2010**, *43*, 10366−10375.

51 K. Yagi, M. Ito, H. Houjou, *Macromol. Rapid Commun.* **2012**, *33*, 540−544.

52 M. T. Nguyen, B. J. Holliday, *Chem. Commun.* **2015**, *51*, 8610−8613.

53 S. Realista, A. S. Viana, B. d. P. Cardoso, A. M. Botelho do Rego, P. D. Vaz, A. I. Melato, P. N. Martinho, M. J. Calhorda, *RSC Adv.* **2015**, *5*, 39495−39504.

54 W. Y. Chan, S. B. Clendenning, A. Berenbaum, A. J. Lough, S. Aouba, H. E. Ruda, I. Manners, *J. Am. Chem. Soc.* **2005**, *127*, 1765−1772.

55 M. Zamora, S. Bruña, B. Alonso, I. Cuadrado, *Macromolecules* **2011**, *44*, 7994−8007.

56 J. Zhang, Y. Yan, J. Chen, W. M. Chance, J. Hayat, Z. Gai, C. Tang, *Chem. Mater.* **2014**, *26*, 3185−3190.

57 Q. Dong, G. Li, H. Wang, P. Wing-Tat Pong, C.-W. Leung, I. Manners, C.-L. Ho, H. Li, W.-Y. Wong, *J. Mater. Chem. C* **2015**, *3*, 734−741.

58 R. Ciganda, H. Gu, P. Castel, P. Zhao, J. Ruiz, R. Hernández, D. Astruc, *Macromol. Rapid Commun.* **2016**, *37*, 105−111.

59 J. A. Paquette, E. R. Sauvé, J. B. Gilroy, *Macromol. Rapid Commun.* **2015**, *36*, 621−626.

60 F. A. Cotton, J. Czuchajowska, *Polyhedron* **1990**, *9*, 2553−2566.

61 P. Mountford, *Chem. Soc. Rev.* **1998**, *27*, 105−115.

62 A. S. Abd-El-Aziz, P. O. Shipman, B. N. Boden, W. S. McNeil, *Prog. Polym. Sci.* **2010**, *35*, 714−836.

63 J. Gwyther, J. B. Gilroy, P. A. Rupar, D. J. Lunn, E. Kynaston, S. K. Patra, G. R. Whittell, M. A. Winnik, I. Manners, *Chem. Eur. J.* **2013**, *19*, 9186−9197.

64 J. H. Niewahner, K. A. Walters, A. Wagner, *J. Chem. Educ.* **2007**, *84*, 477.

65 R. Bernard, C. Barsu, P. L. Baldeck, C. Andraud, D. Cornu, J.-P. Scharff, P. Miele, *Chem. Commun.* **2008**, 3765−3767.

66 C. L. Bailey, R. D. Bereman, D. P. Rillema, R. Nowak, *Inorg. Chem.* **1984**, *23*, 3956−3960.

67 N. Fomina, S. E. Bradforth, T. E. Hogen-Esch, *Macromolecules* **2009**, *42*, 6440−6447.

68 T.-A. Chen, X. Wu, R. D. Rieke, *J. Am. Chem. Soc.* **1995**, *117*, 233−244.

69 F. C. McElroy, J. C. Dabrowiak, *J. Am. Chem. Soc.* **1976**, *98*, 7112−7113.

70 C. L. Bailey, R. D. Bereman, D. P. Rillema, R. Nowak, *Inorg. Chem.* **1986**, *25*, 933−938.

71 D. Kim, E. Kim, J. Byun, J. Choi, H. Na, Y. Park, *J. Coord. Chem.* **2002**, *55*, 505−516.

72 N. A. M. Barakat, B. Kim, C. Yi, Y. Jo, M.-H. Jung, K. H. Chu, H. Y. Kim, *J. Phys. Chem. C* **2009**, *113*, 19452−19457.

73 K. Lian, S. J. Thorpe, D. W. Kirk, *Electrochim. Acta* **1992**, *37*, 169−175.

74 R. Xu, T. Xie, Y. Zhao, Y. Li, *Nanotechnology* **2007**, *18*, 055602.

75 J. Chang, J. Sun, C. Xu, H. Xu, L. Gao, *Nanoscale* **2012**, *4*, 6786−6791.

Supporting Information

Synthesis, Characterization, and Pre-Ceramic Properties of π-Conjugated Polymers Based on Ni(II) Complexes of Goedken's Macrocycle

Joseph A. Paquette and Joe B. Gilroy*

Department of Chemistry and The Centre for Advanced Materials and Biomaterials Research (CAMBR), The University of Western Ontario, 1151 Richmond St. N., London, Ontario, Canada, N6A 5B7.

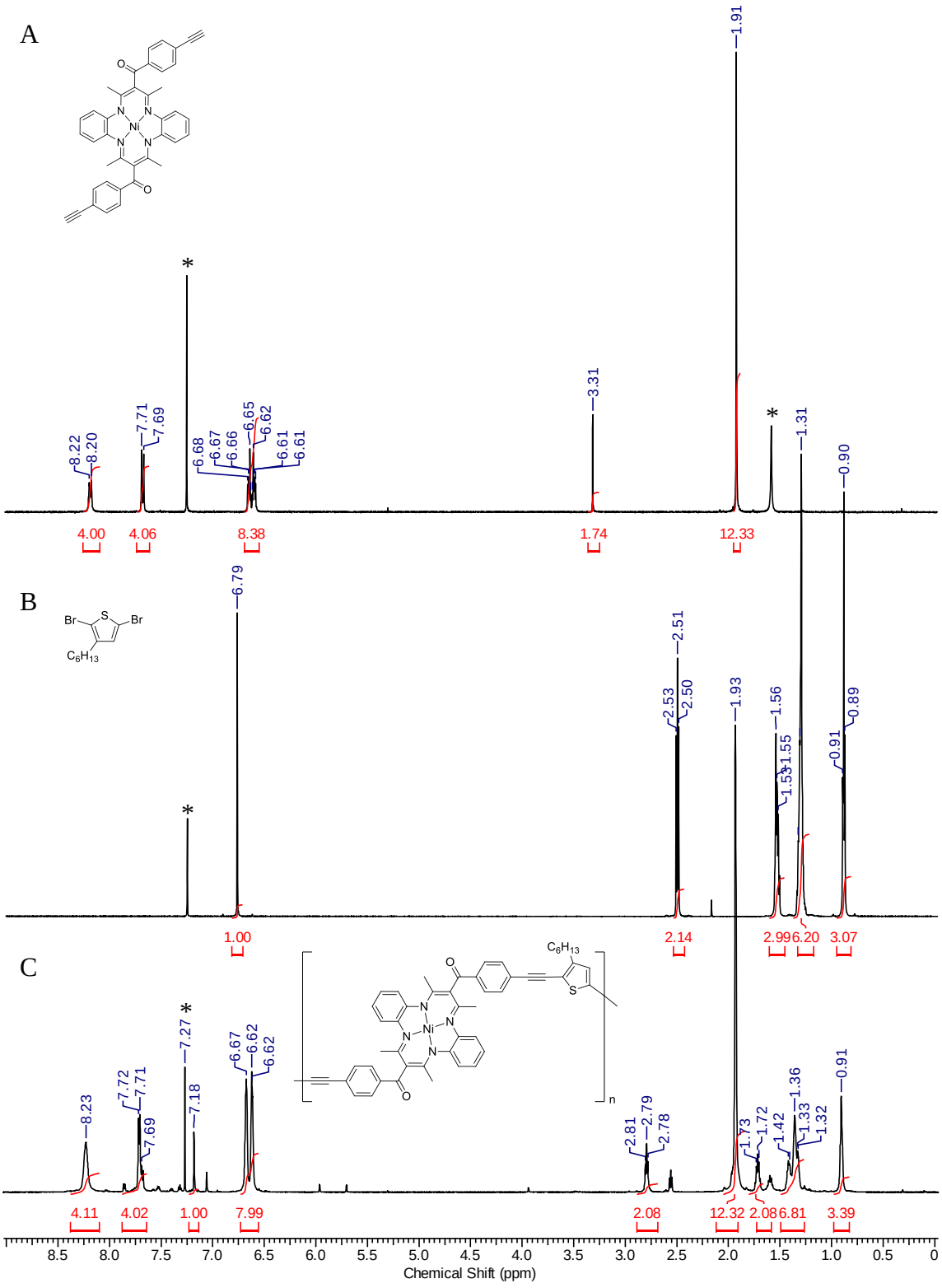

Figure S1. ^{1}H NMR spectra of A) **5**, B) 1,4-dibromo-3-hexylthiophene, and C) copolymer **6T** in $CDCl_3$. Asterisks denote residual solvent signals.

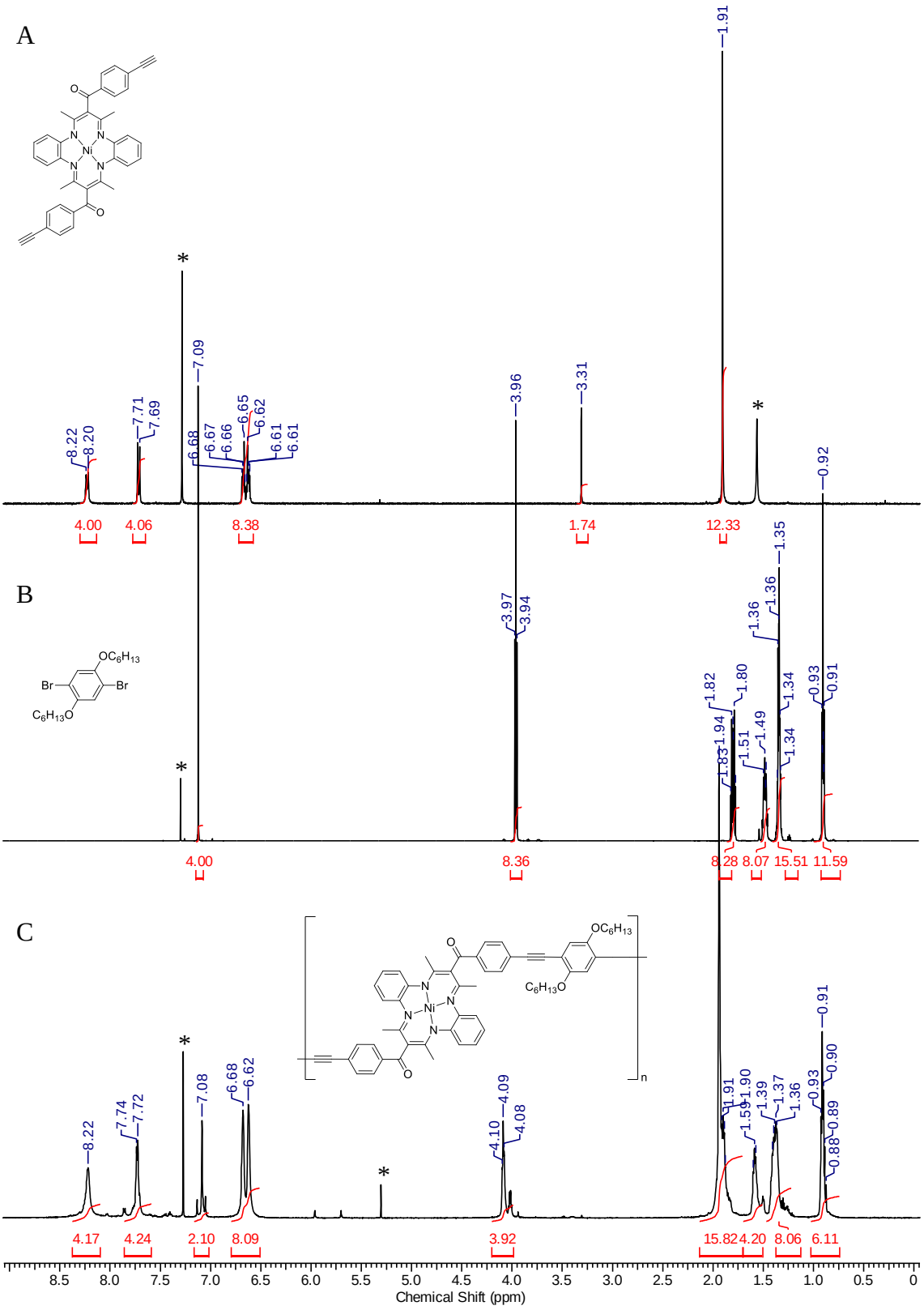

Figure S2. ^{1}H NMR spectra of A) **5**, B)1,4-dibromo-2,5-bis(hexyloxy)benzene, and C) copolymer **6B** in $CDCl_3$. Asterisks denote residual solvent signals.

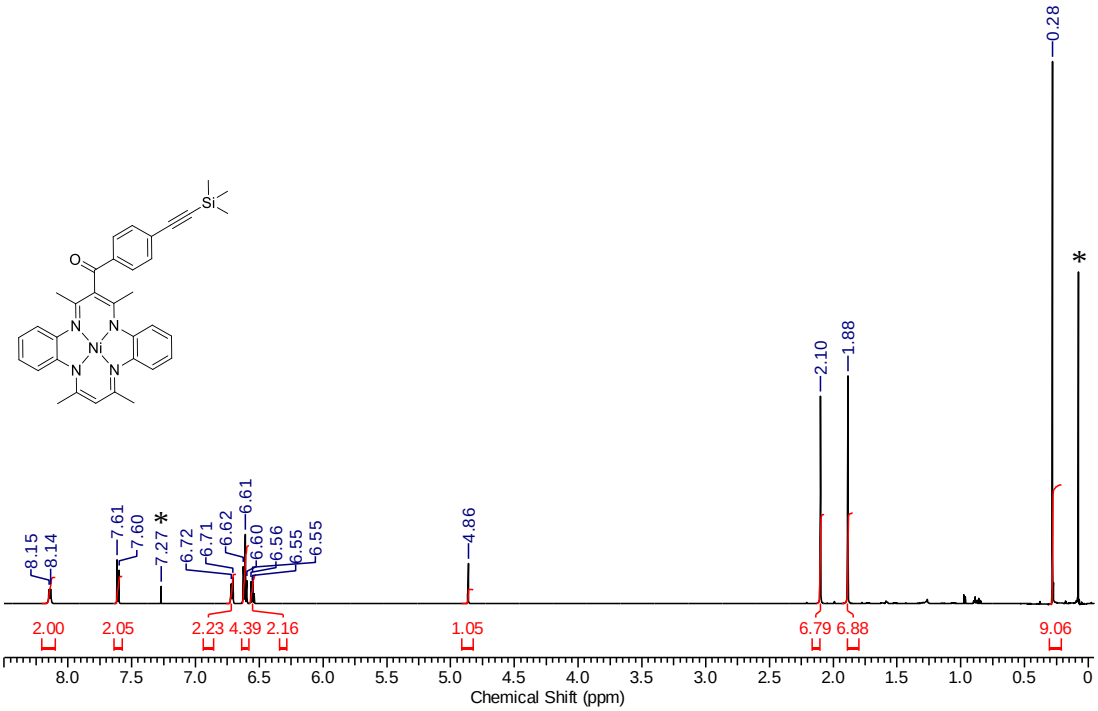

Figure S3. ^{1}H NMR spectrum of **8** in $CDCl_3$. Asterisks denote residual solvent and grease signals.

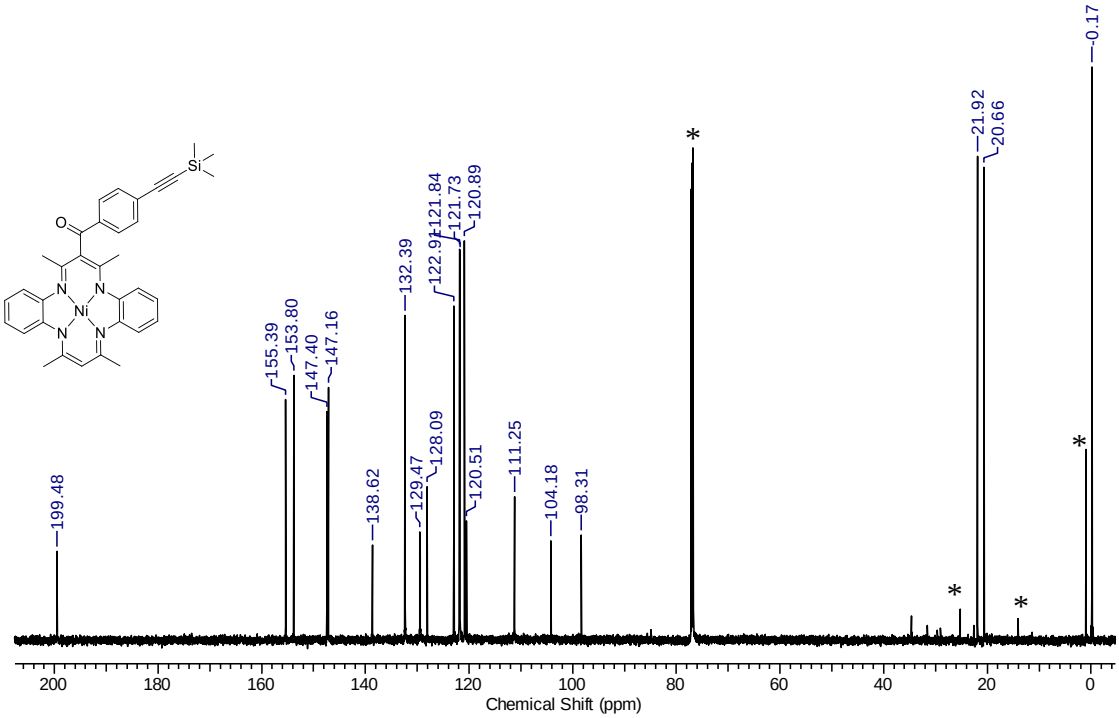

Figure S4. $^{13}C\{^{1}H\}$ NMR spectrum of **8** in $CDCl_3$. Asterisks denote solvent and grease signals.

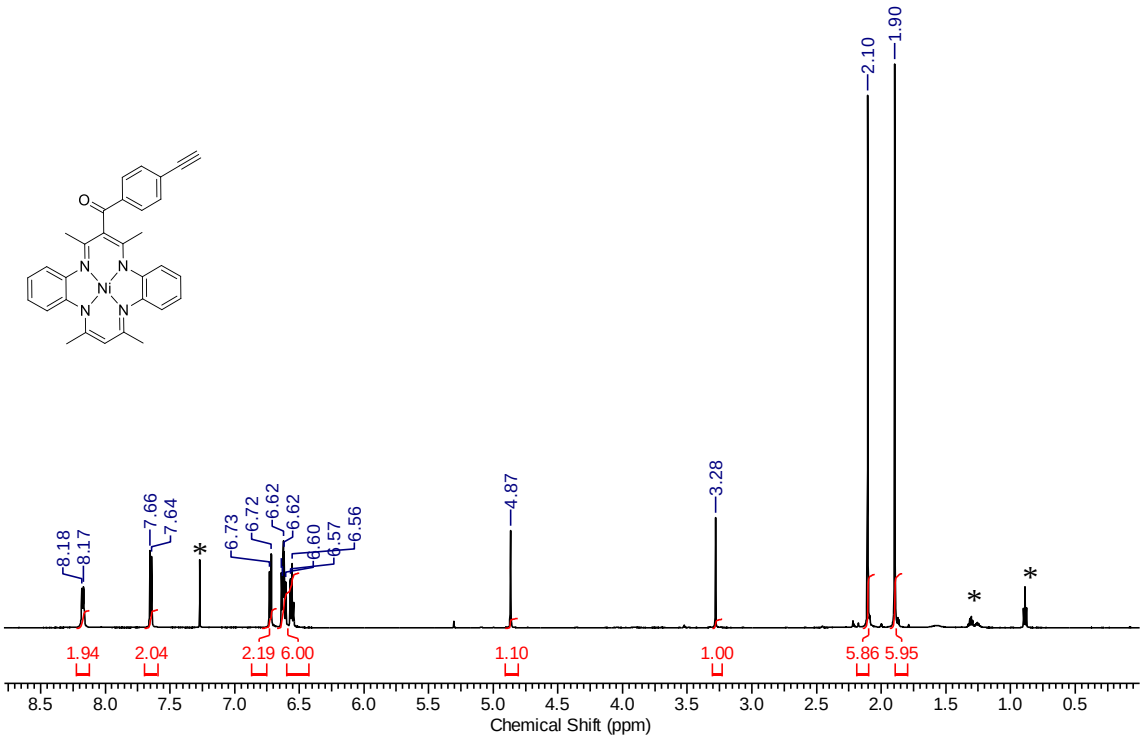

Figure S5. ^{1}H NMR spectrum of **10** in $CDCl_3$. Asterisks denote residual solvent signals.

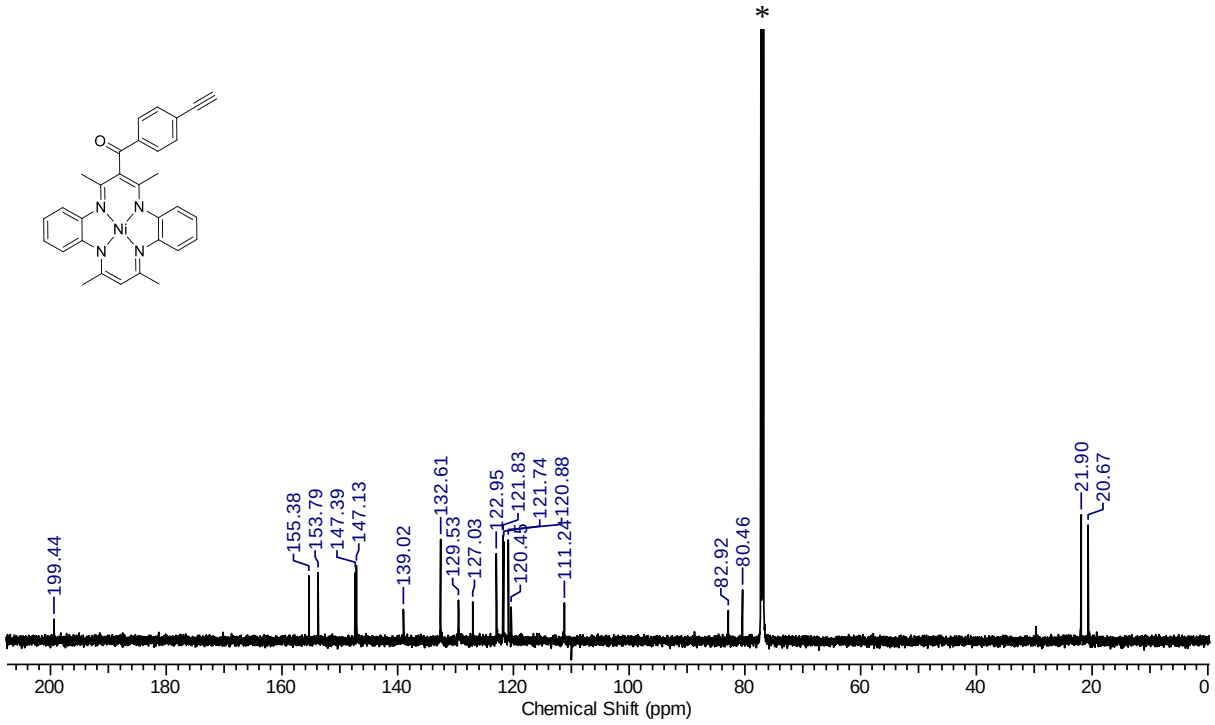

Figure S6. $^{13}C\{^{1}H\}$ NMR spectrum of **10** in $CDCl_3$. Asterisk denotes solvent signal.

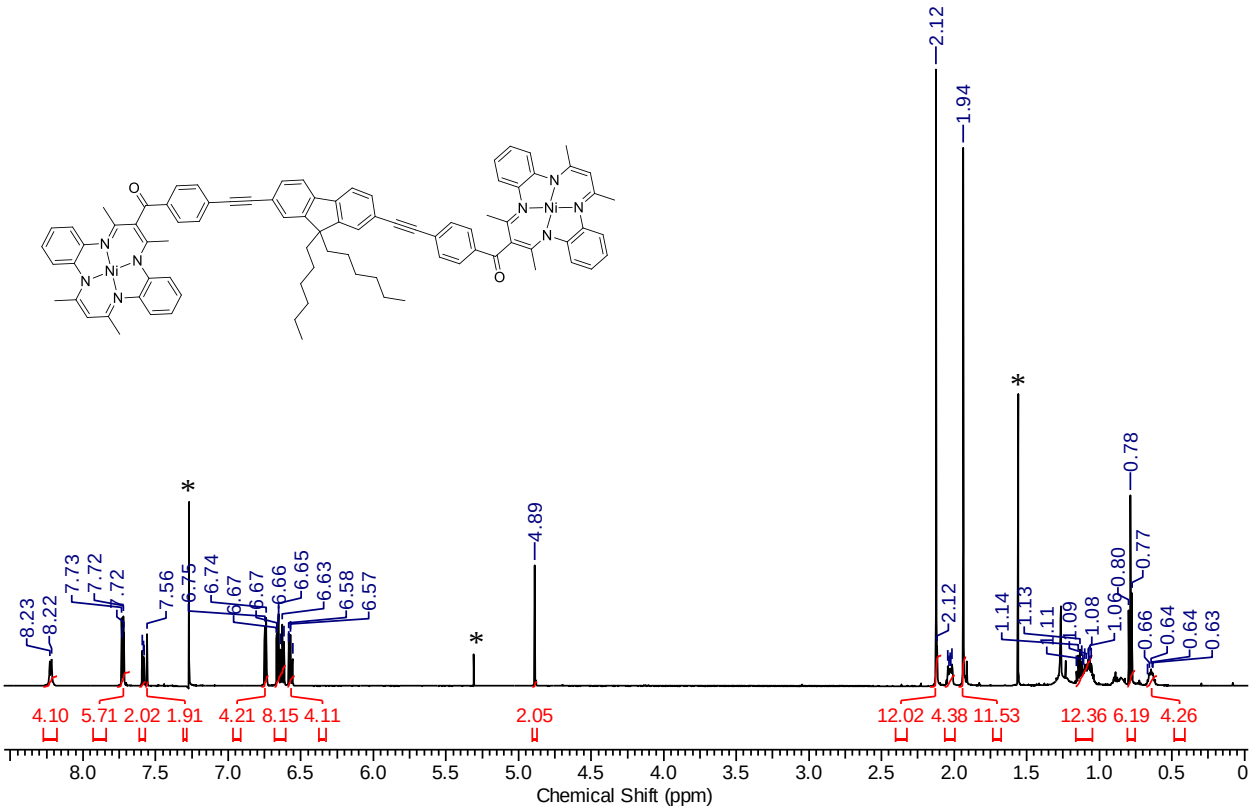

Figure S7. ^{1}H NMR spectrum of **11** in $CDCl_3$. Asterisks denote residual solvent signals.

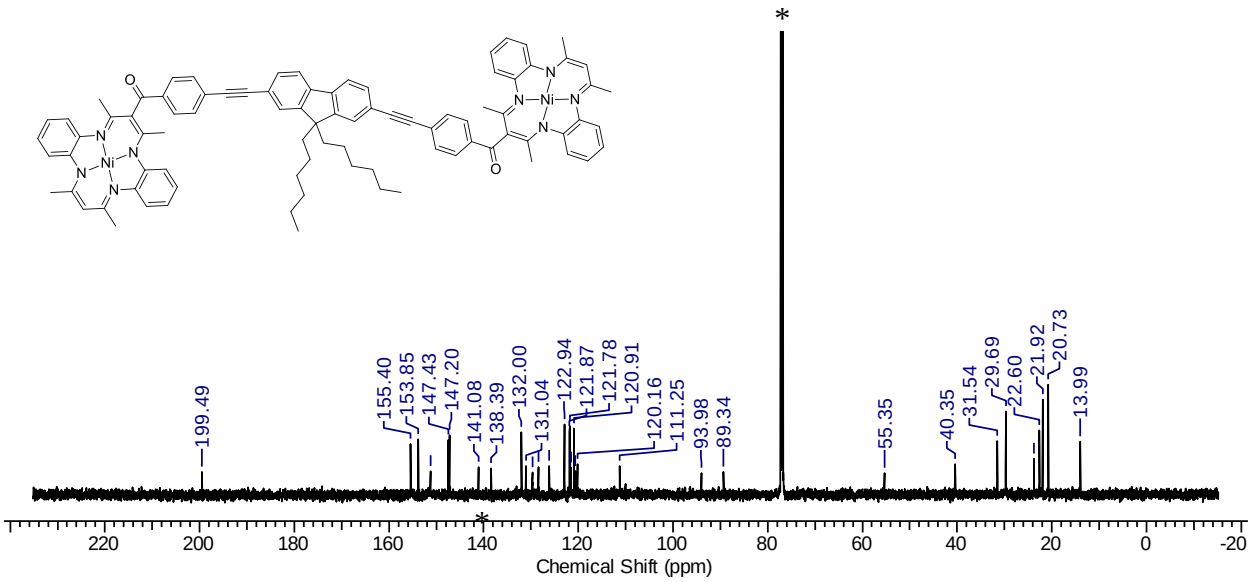

Figure S8. $^{13}C\{^{1}H\}$ NMR spectrum of **11** in $CDCl_3$. Asterisk denotes solvent signal.

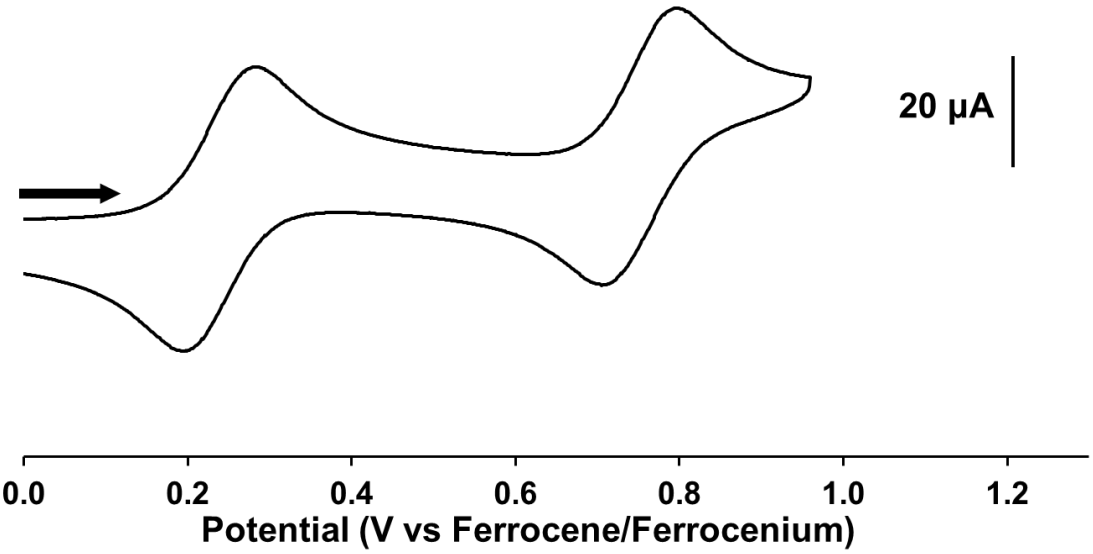

Figure S9. Cyclic voltammagram of model compound **12** recorded at a scan rate of 100 mV s^{-1} in a CH_2Cl_2 solution containing 1×10^{-3} M analyte and 0.1 M [*n*Bu_4N][PF_6] as supporting electrolyte.

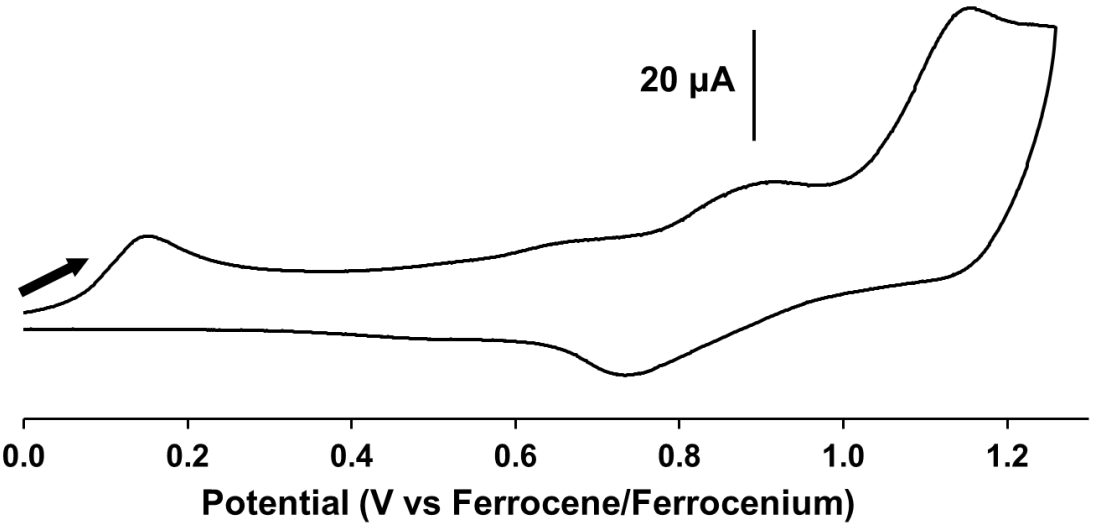

Figure S10. Cyclic voltammagram of model compound **11** recorded at a scan rate of 100 mV s^{-1} in a CH_2Cl_2 solution containing 1×10^{-3} M analyte and 0.1 M [*n*Bu_4N][PF_6] as supporting electrolyte.

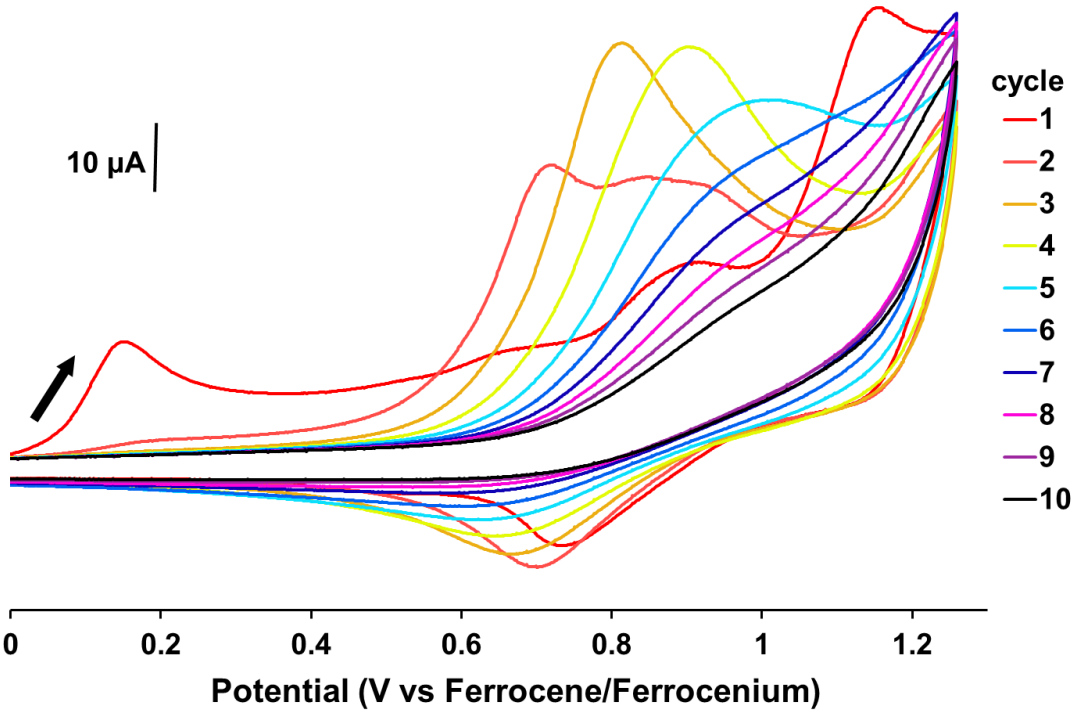

Figure S11. Cyclic voltammagrams of **11** cycled 10 times and recorded at a scan rate of 250 mV s^{-1} in a CH_2Cl_2 solution containing 1 × 10^{-3} M analyte and 0.1 M [*n*Bu_4N][PF_6] as supporting electrolyte.

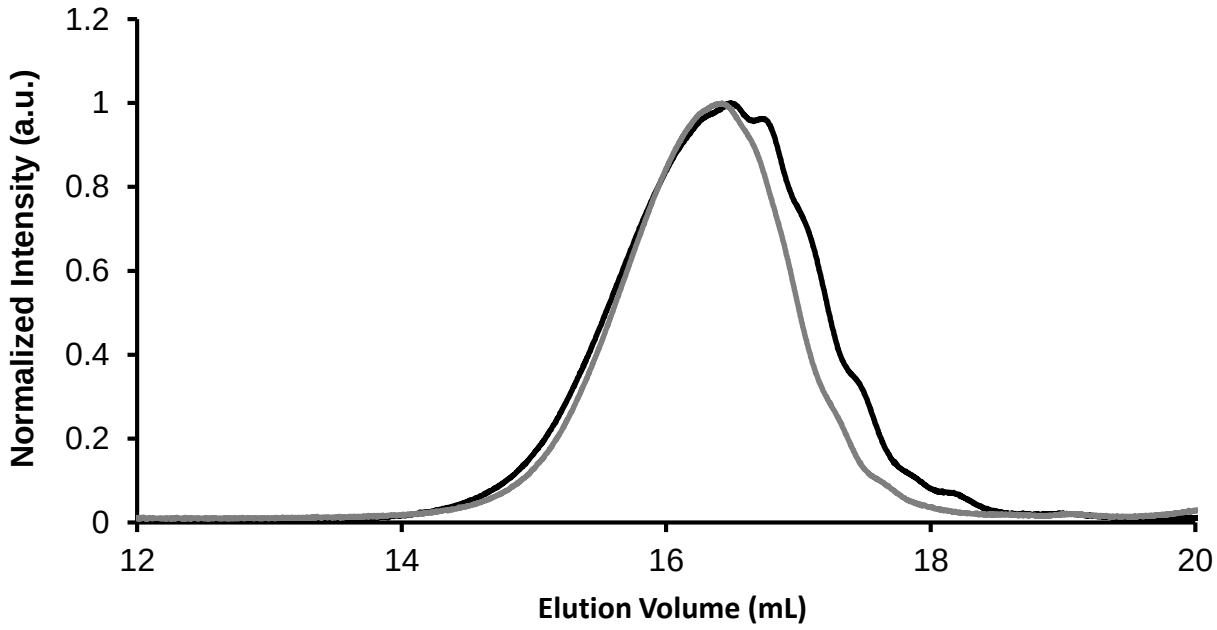

Figure S12. GPC traces for **6F** (black) and **6F-[$Co_2(CO)_6$]$_2$** (grey).

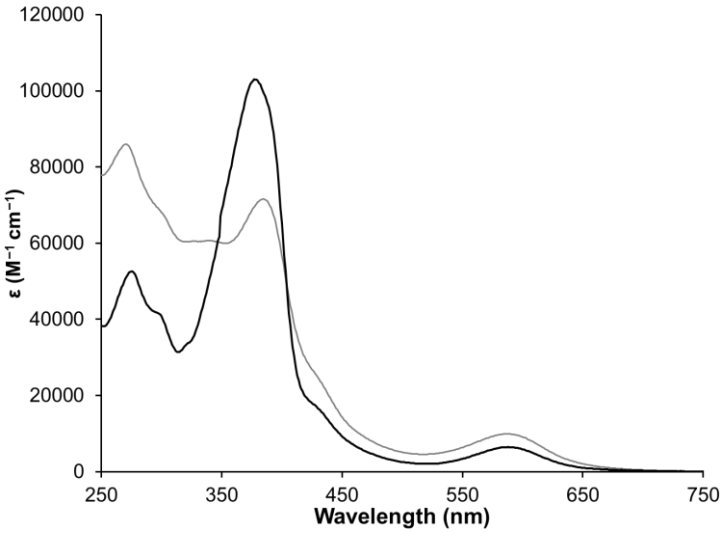

Figure S13. UV-vis absorption spectra of **6F** (black) and **6F-[$Co_2(CO)_6$]$_2$** (grey) in CH_2Cl_2.

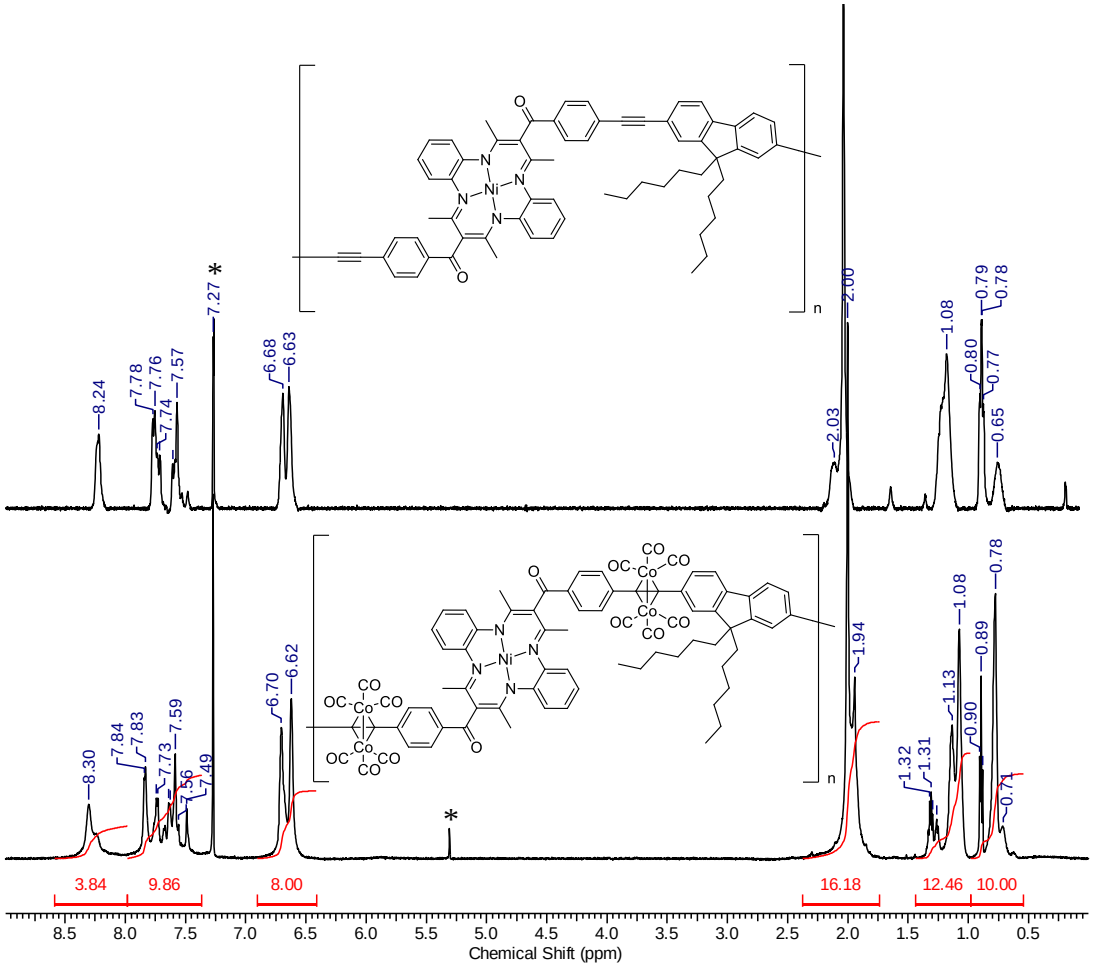

Figure S14. ^{1}H NMR spectrum of **6F** and **6F-[$Co_2(CO)_6$]$_2$** in $CDCl_3$. Asterisks denote residual solvent signals.

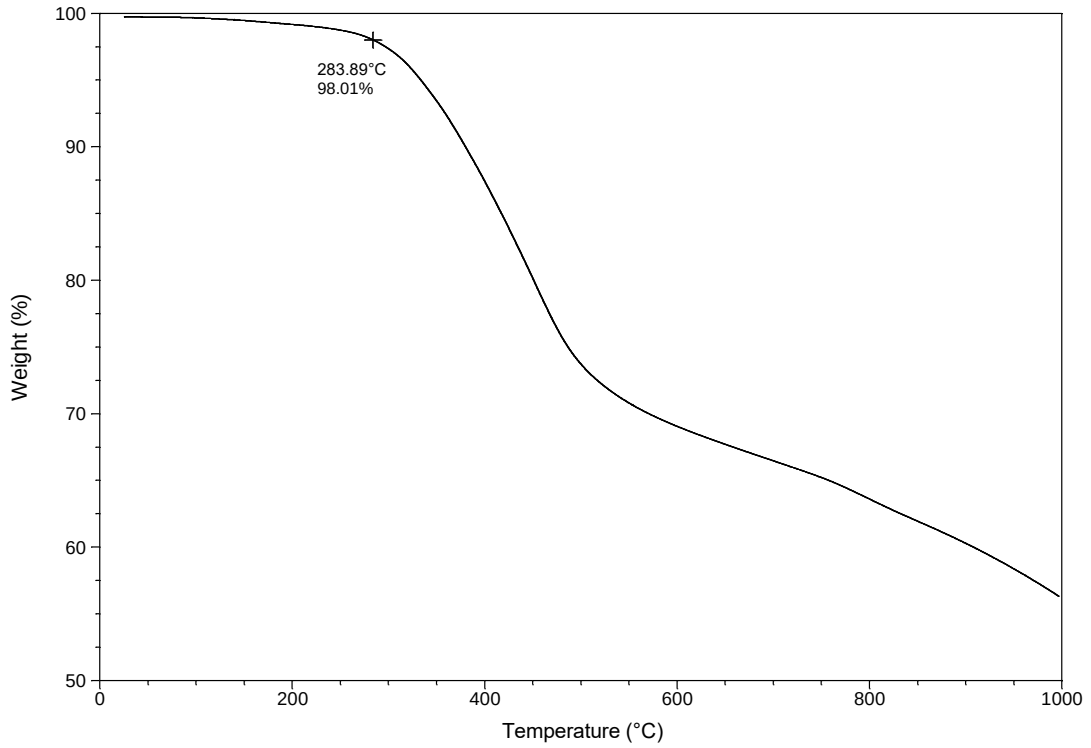

Figure S15. TGA data for **6T**.

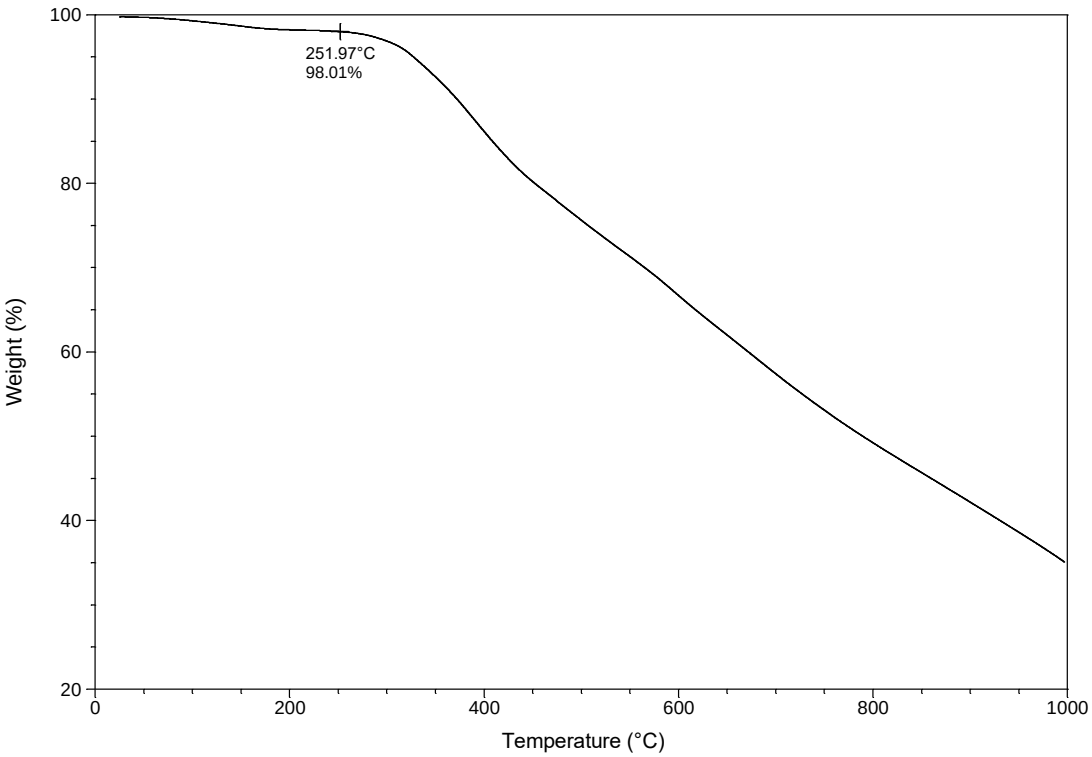

Figure S16. TGA data for **6B**.

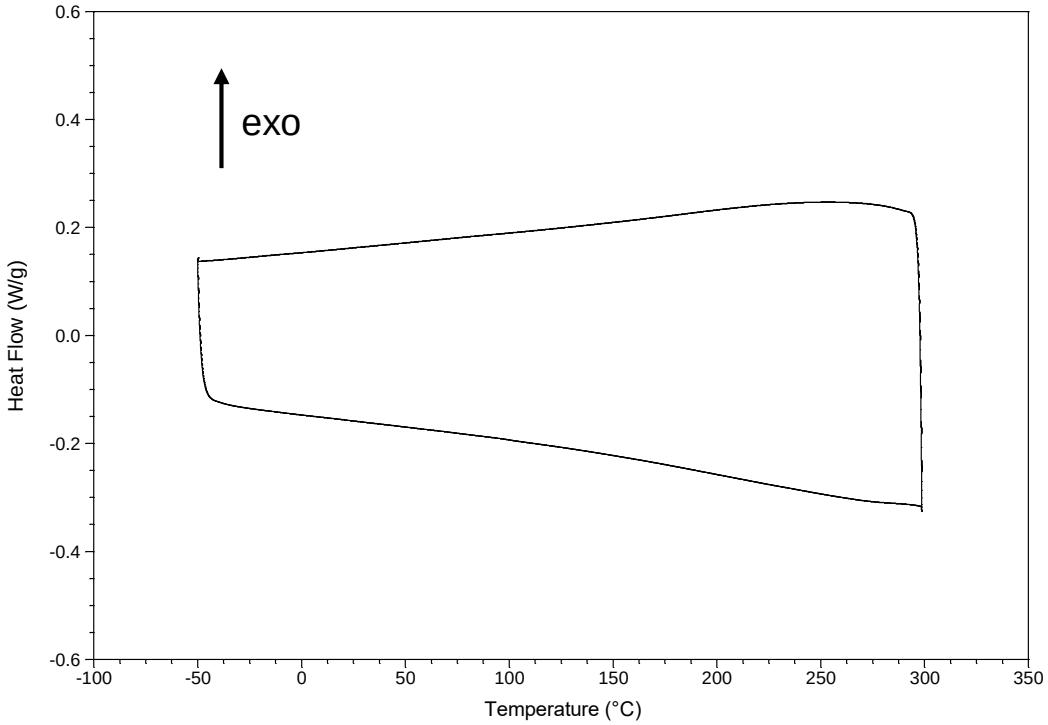

Figure S17. DSC trace for **6F**. The second heating/cooling cycle is shown.

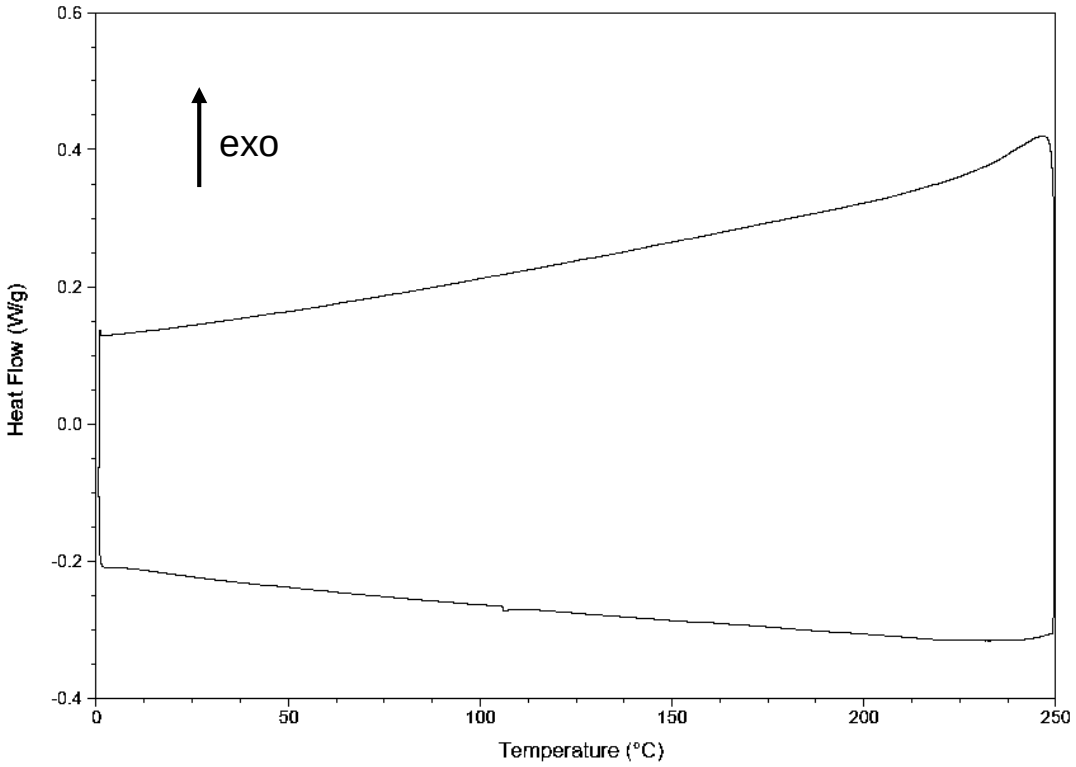

Figure S18. DSC trace for **6T**. The second heating/cooling cycle is shown.

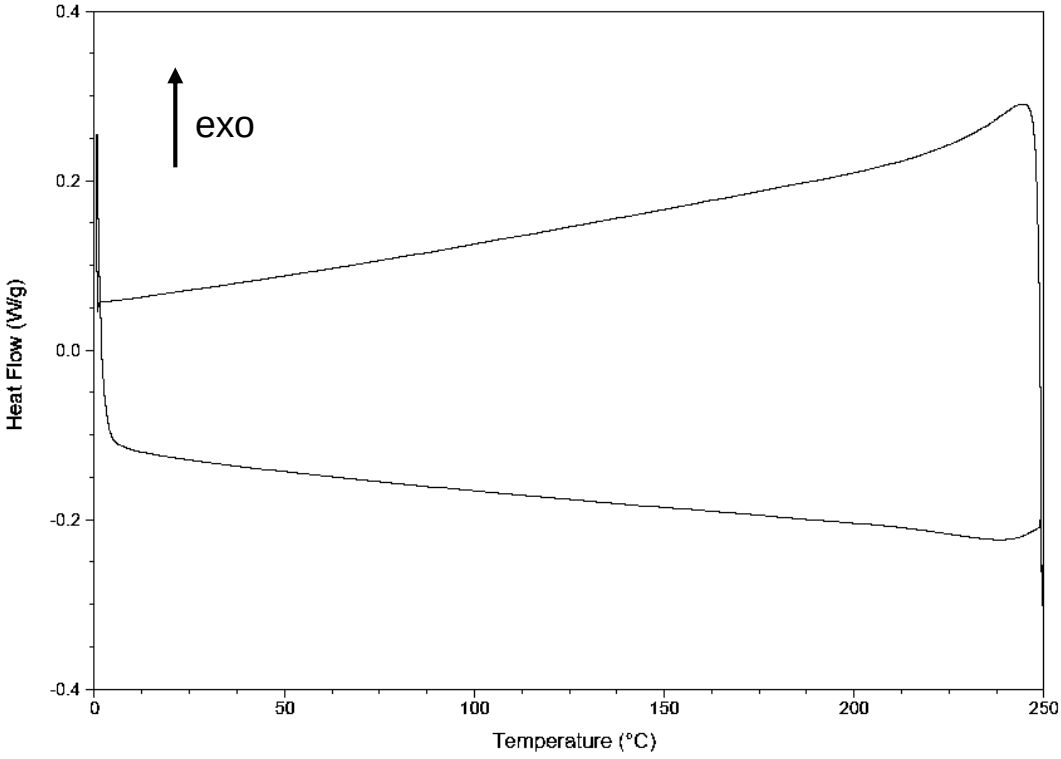

Figure S19. DSC trace for **6B**. The second heating/cooling cycle is shown.

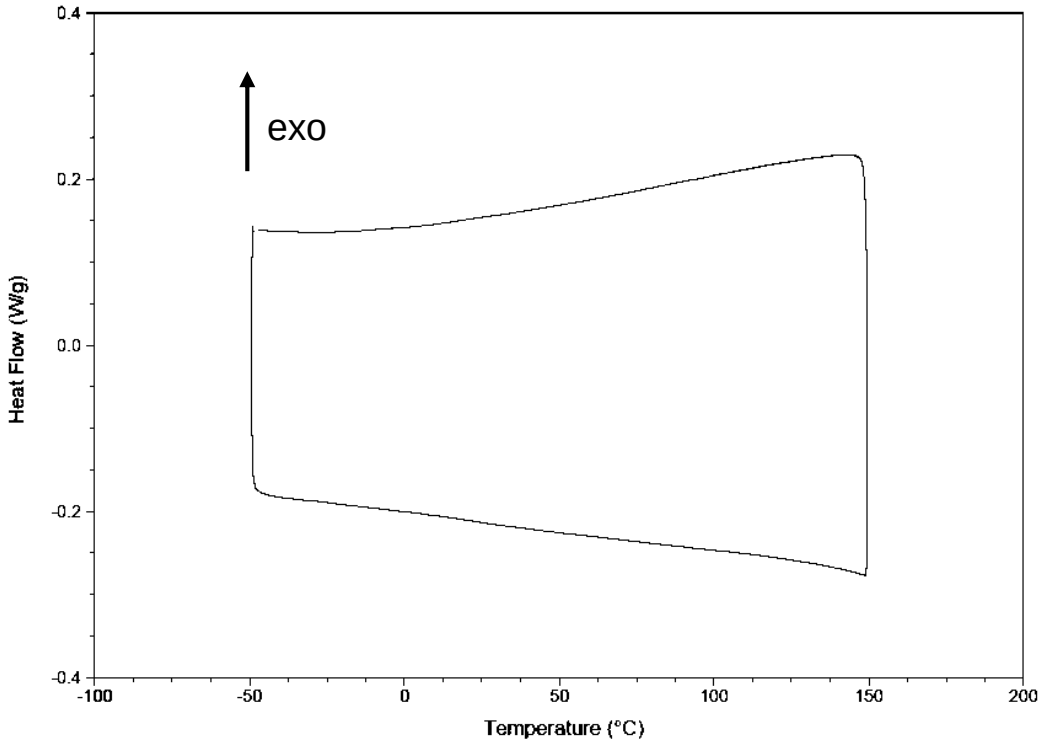

Figure S20. DSC trace for **6F-[$Co_2(CO)_6$]**. The second heating/cooling cycle is shown.

Figure S21. SEM of a cross-section of a thin film prepared by drop casting **6F-[Co$_2$(CO)$_6$]$_2$** onto a silicon wafer.

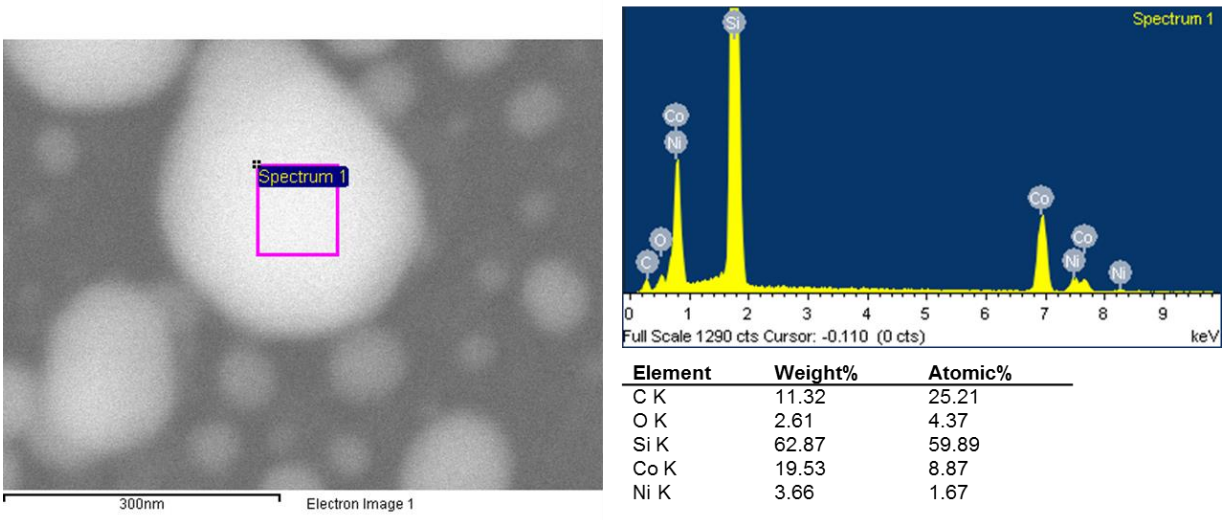

Element	Weight%	Atomic%
C K	11.32	25.21
O K	2.61	4.37
Si K	62.87	59.89
Co K	19.53	8.87
Ni K	3.66	1.67

Figure S22. EDX spectroscopy data collected from the nanomaterials produced from the pyrolysis of thin film of **6F-[Co$_2$(CO)$_6$]$_2$** on a silicon wafer.